Cell Reports

Article

Setd1a Insufficiency in Mice Attenuates Excitatory Synaptic Function and Recapitulates Schizophrenia-Related Behavioral Abnormalities

Graphical Abstract

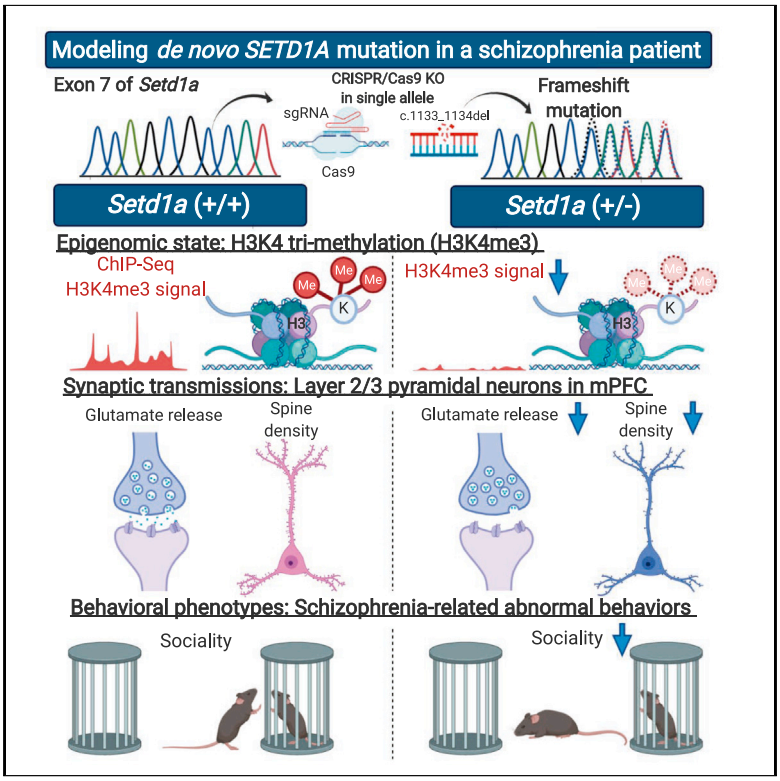

Highlights

- *Setd1a* (+/−) mice mimicking a frameshift mutation of a SCZ patient are generated
- *Setd1a* (+/−) mice display various abnormal behaviors relevant to features of SCZ
- Postsynaptic SETD1A is crucial for excitatory synaptic function and structure
- *Setd1a* in layer 2/3 pyramidal neurons of mPFC is involved in mouse social behavior

Authors

Kenichiro Nagahama, Kazuto Sakoori, Takaki Watanabe, ..., Atsu Aiba, Naofumi Uesaka, Masanobu Kano

Correspondence

uesaka.cnb@tmd.ac.jp (N.U.), mkano-tky@m.u-tokyo.ac.jp (M.K.)

In Brief

Nagahama et al. demonstrate that mimicking a *de novo* mutation of the schizophrenia-risk gene *SETD1A* in mice induces various abnormal behaviors relevant to schizophrenia. *Setd1a* in postsynaptic neurons positively regulates excitatory synaptic transmission and structure in the medial prefrontal cortex through histone modification and regulating the expression of diverse synaptic genes.

Nagahama et al., 2020, Cell Reports *32*, 108126
September 15, 2020
https://doi.org/10.1016/j.celrep.2020.108126

CellPress

Cell Reports

CellPress
OPEN ACCESS

Article

Setd1a Insufficiency in Mice Attenuates Excitatory Synaptic Function and Recapitulates Schizophrenia-Related Behavioral Abnormalities

Kenichiro Nagahama,[1,2] Kazuto Sakoori,[1] Takaki Watanabe,[1,2] Yusuke Kishi,[3] Keita Kawaji,[3] Michinori Koebis,[4] Kazuki Nakao,[4] Yukiko Gotoh,[2,3] Atsu Aiba,[4] Naofumi Uesaka,[1,2,5,*] and Masanobu Kano[1,2,6,*]

[1]Department of Neurophysiology, Graduate School of Medicine, The University of Tokyo, Tokyo 113-0033, Japan
[2]International Research Center for Neurointelligence (WPI-IRCN), The University of Tokyo Institutes for Advanced Study, The University of Tokyo, Tokyo 113-0033, Japan
[3]Laboratory of Molecular Biology, Graduate School of Pharmaceutical Sciences, The University of Tokyo, Tokyo 113-0033, Japan
[4]Laboratory of Animal Resources, Center for Disease Biology and Integrated Medicine, Graduate School of Medicine, The University of Tokyo, Tokyo 113-0033, Japan
[5]Graduate School of Medical and Dental Sciences, Tokyo Medical and Dental University, Tokyo 113-8510, Japan
[6]Lead Contact
*Correspondence: uesaka.cnb@tmd.ac.jp (N.U.), mkano-tky@m.u-tokyo.ac.jp (M.K.)
https://doi.org/10.1016/j.celrep.2020.108126

SUMMARY

SETD1A encodes a histone methyltransferase whose *de novo* mutations are identified in schizophrenia (SCZ) patients and confer a large increase in disease risk. Here, we generate *Setd1a* mutant mice carrying the frameshift mutation that closely mimics a loss-of-function variant of SCZ. Our *Setd1a* (+/−) mice display various behavioral abnormalities relevant to features of SCZ, impaired excitatory synaptic transmission in layer 2/3 (L2/3) pyramidal neurons of the medial prefrontal cortex (mPFC), and altered expression of diverse genes related to neurodevelopmental disorders and synaptic functions in the mPFC. RNAi-mediated *Setd1a* knockdown (KD) specifically in L2/3 pyramidal neurons of the mPFC only recapitulates impaired sociality among multiple behavioral abnormalities of *Setd1a* (+/−) mice. Optogenetics-assisted selective stimulation of presynaptic neurons combined with *Setd1a* KD reveals that *Setd1a* at postsynaptic site is essential for excitatory synaptic transmission. Our findings suggest that reduced SETD1A may attenuate excitatory synaptic function and contribute to the pathophysiology of SCZ.

INTRODUCTION

Schizophrenia (SCZ) is a common psychiatric disorder with a complex etiology whose associated molecular pathophysiology is poorly understood (Insel, 2010; Owen et al., 2016). Studies with genome-wide association study (GWAS) and whole-exome sequencing have demonstrated a strong relationship between SCZ-susceptible genes and synaptic function (Fromer et al., 2014; Hayashi-Takagi, 2017; Schizophrenia Working Group of the Psychiatric Genomics Consortium, 2014). Impairment of inhibitory synaptic transmission is also suggested in brain samples from SCZ patients (Gonzalez-Burgos et al., 2010; Lewis et al., 2005). As for the cell types involved in SCZ pathophysiology, neocortical pyramidal neurons and inhibitory interneurons were identified by the analysis of gene datasets from single-cell RNA sequencing (scRNA-seq) (Skene et al., 2018). Several strains of mouse model for the study of SCZ were reported to exhibit synaptic dysfunction (Earls et al., 2010; Fénelon et al., 2013; Hayashi-Takagi et al., 2010; Marissal et al., 2018; Mei and Xiong, 2008) and reduced spine density in pyramidal neurons (Hayashi-Takagi et al., 2010; Jones et al., 2011; Mei and Xiong, 2008) similar to what was observed in SCZ postmortem brains (Glausier and Lewis, 2013; Konopaske et al., 2014). These lines of evidence suggest that both functional and structural deficits in synapses are present in SCZ patients. Although SCZ is considered a highly polygenetic disorder (Owen et al., 2016), the identification of SCZ risk genes whose mutations are causally related to disease onset and elucidation of their roles in synaptic function in mice will greatly facilitate the understanding of molecular, cellular, and circuit mechanisms underlying the pathophysiology of SCZ.

Epigenomic mechanisms, including histone modification, are thought to be involved in the pathogenesis of psychiatric disorders (Akbarian and Nestler, 2013; Huang et al., 2007; Shorter and Miller, 2015; Sun et al., 2016). Recently, rare *de novo* mutations were reported in *SETD1A*, a gene that encodes histone 3 lysine 4 (H3K4) tri-methyltransferase (Bledau et al., 2014; Dillon et al., 2005), in some patients with SCZ (Singh et al., 2016; Takata et al., 2014, 2016). *SETD1A* is the gene whose loss-of-function (LoF) mutation is considered to be the main cause of SCZ symptoms, at least in these patients. Bledau et al. (2014) generated *Setd1a* knockout mice by inserting the FLP

recombination target (FRT)-flanked *LacZ* trapping cassette and a promoter-driven neo cassette in the upstream of exon 4 of the *Setd1a* gene, which led to premature termination of the transcript and produced a null allele of *Setd1a*. Whereas *Setd1a* homozygous knockout mice were lethal after embryonic day 7.5 (E7.5) (Bledau et al., 2014), Mukai et al. (2019) reported recently that *Setd1a* heterozygous knockout (*Setd1a*$^{+/-}$) mice exhibited alterations in axon branching and synaptic dynamics accompanied by working memory deficits. Moreover, *Setd1a*$^{+/-}$ mice were altered in transcriptional regulation in tissues of the medial prefrontal cortex (mPFC) (Mukai et al., 2019), a brain area thought to be involved in SCZ (Pomarol-Clotet et al., 2010). However, it remains unknown whether mutations that closely mimic the *de novo* LoF variants of *SETD1A* found in SCZ patients induce SCZ-related molecular, synaptic, and behavioral phenotypes in mice.

To address these questions, we generated *Setd1a* heterozygous mutant mice (*Setd1a* (+/−)) carrying a frameshift mutation in exon 7 of *Setd1a*, which mimics a *de novo* mutation of *SETD1A* in a SCZ patient. We performed comprehensive behavioral analyses, electrophysiological and morphological examinations of synaptic function and structure in layer 2/3 (L2/3) pyramidal neurons of the mPFC, and gene expression analysis of mPFC tissues. We also performed RNAi-mediated *Setd1a* knockdown (KD) in L2/3 pyramidal neurons of the mPFC and conducted comprehensive analyses of mouse behaviors and examination of synaptic function. The results presented below show that *Setd1a* at the postsynaptic site is required for maintaining excitatory synaptic function and structure in L2/3 pyramidal neurons of the mPFC, and the disruption of *Setd1a* causes behavioral abnormalities relevant to features of SCZ in mice.

RESULTS

Generation of *Setd1a* (+/−) Mice Carrying a Mutation Analogous to That of a SCZ Patient

To investigate molecular and neural circuit mechanisms underlying SCZ, we require mouse lines carrying genetic mutations analogous to those identified in SCZ patients (Diamantopoulou and Gogos, 2019). We generated mice with a *Setd1a* mutation mimicking one of the patients with reported LoF variants of *SETD1A* (Singh et al., 2016; Takata et al., 2014) by means of clustered regularly interspaced short palindromic repeats and the associated proteins (CRISPR-Cas9) system. We introduced a frameshift mutation in the same exon (2-base deletion on exon 7) as reported in a patient with typical SCZ symptoms (Figures 1A–1C). We obtained only *Setd1a* (+/−) and wild-type (*Setd1a* (+/+)) mice from genome-edited embryos, probably because our *Setd1a* (−/−) mice are embryonic lethal, similar to the previously reported *Setd1a* homozygous knockout mice (Bledau et al., 2014). We confirmed the SETD1A protein level became almost half in the mPFC of our *Setd1a* (+/−) mice compared to our *Setd1a* (+/+) mice (Figure 1D). The birth rate of *Setd1a* (+/−) pups was smaller than that of *Setd1a* (+/+) littermates (Figure 1E), as reported previously (Bledau et al., 2014), whereas body weight at 2 months of age was identical between the 2 genotypes (Figure 1F), suggesting an involvement of SETD1A in mouse embryonic development. The number of NeuN^{+} cells from L1 to deep layers were comparable between the 2 mouse strains (Figures 1G and 1H), suggesting that the layer structure of the PFC of *Setd1a* (+/−) mice was normal. These results demonstrate that *Setd1a* (+/−) mice exhibit reduced expression of SETD1A through the mutation that is analogous to that reported in a SCZ patient; this may impair embryonic development without altering the gross morphology of the mPFC.

Setd1a (+/−) Mice Show SCZ-Related Abnormal Behaviors

To investigate the roles of *Setd1a* in mouse behavior, we conducted comprehensive behavioral tests (Table S1). In the open field test, we found that *Setd1a* (+/−) mice showed severe hyperactivity at days 1 and 2 (Figures 2A and 2B). In the prepulse inhibition (PPI) test, *Setd1a* (+/−) mice did not display statistically significant impairment compared to *Setd1a* (+/+) mice (Figure 2C). The magnitude of startle responses to sounds from 70 to 120 dB was identical between genotypes (Figure S1A), indicating that auditory function and startle response were intact in *Setd1a* (+/−) mice. The results of the PPI test suggest a barely intact sensorimotor gating in *Setd1a* (+/−) mice. In the sociality test, *Setd1a* (+/−) mice spent significantly shorter time around the novel mouse cage than did the *Setd1a* (+/+) mice (Figure 2E), although the difference in the social preference index between genotypes did not reach the statistically significant level (Figure 2F). In the reciprocal social interaction test, the number of active contacts with a novel mouse was significantly reduced in *Setd1a* (+/−) mice (Figures 2G and 2H). These results collectively indicate that sociality is impaired and motivation of social interaction is reduced in *Setd1a* (+/−) mice.

We also evaluated working memory and the ability to recognize a novel object, since deficit in cognitive function is a major feature of SCZ (Barch and Ceaser, 2012). In the Y-maze spontaneous alteration test, the total number of entries into the arms was not significantly changed (Figures 2I), whereas the percentage of alteration to enter three different arms was decreased in *Setd1a* (+/−) mice (Figure 2J). Furthermore, in the Y-maze delayed alteration test, the percentage of correct responses during training was significantly lower in *Setd1a* (+/−) mice than in *Setd1a* (+/+) mice (Figure S1B). The percentage of correct responses at each delay time was also significantly lower in *Setd1a* (+/−) mice than in *Setd1a* (+/+) mice (Figure S1C), indicating a significant reduction in the correct responses of *Setd1a* (+/−) mice. These results suggest that *Setd1a* (+/−) mice showed impaired working memory, which is consistent with the behavioral results of Mukai et al. (2019). In the novel object recognition test, recognizing a novel object was lower at 1 h in *Setd1a* (+/−) mice, but not at 24 h, after the training (Figures 2K and 2L), indicating impaired recognition of novel objects in *Setd1a* (+/−) mice.

Next, we assessed avoidance behaviors from aversive conditions. In the tail suspension test, *Setd1a* (+/−) mice showed a reduced latency to immobility, while the ratio of immobility was comparable between genotypes during trials, suggesting an impaired avoidance behavior (Figures 2M and 2N). In the light/dark transfer test, the latency to enter the light box for the first time was not significantly different (Figure 2O) and

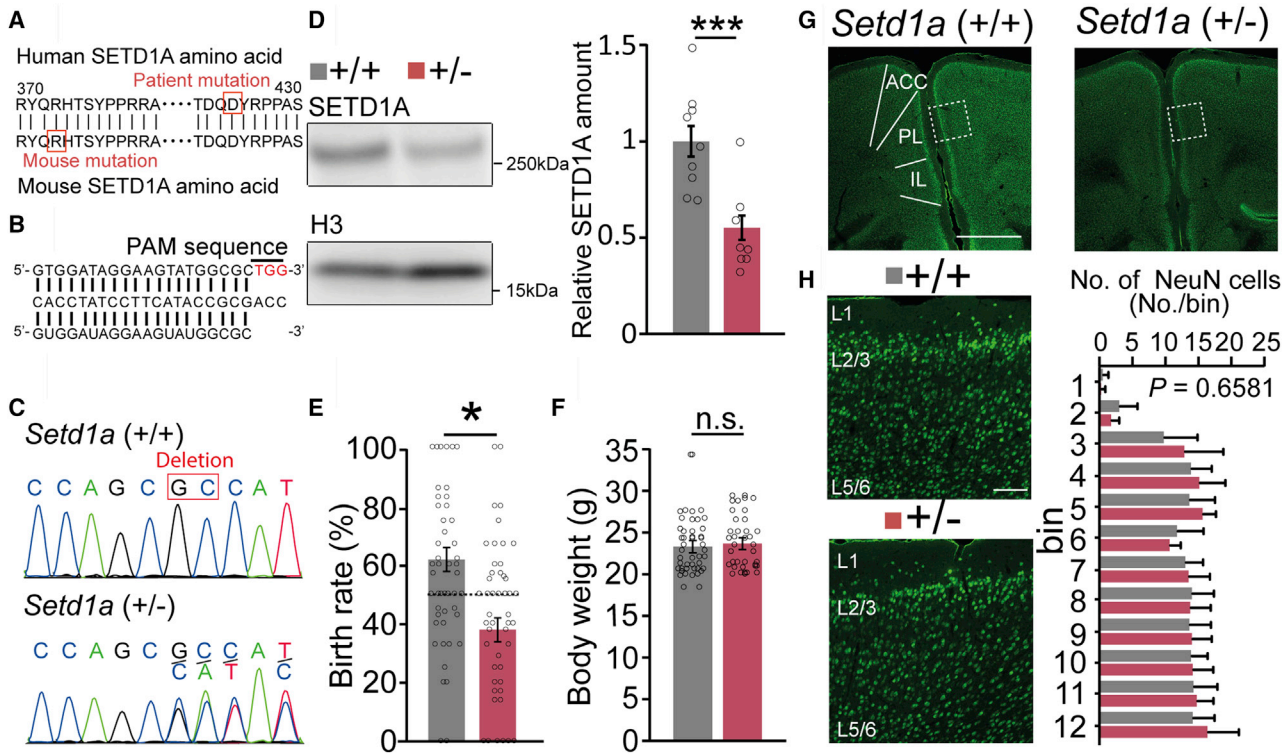

Figure 1. Generation of *Setd1a* (+/−) Mice by CRISPR-Cas9 System

(A) Alignment of amino acid sequences of SETD1A from human and mouse showing the frameshift mutation identified in a SCZ patient (top) and the mutation introduced into mouse (bottom).

(B) Single-guide RNA (sgRNA) sequence targeting exon 7, in which the frameshift mutation shown in (A) was found in a SCZ patient.

(C) Signal intensity of DNA sequencing from *Setd1a* (+/+) and *Setd1a* (+/−) mice. A 2-nt deletion causing a frameshift mutation was inserted into the targeted exon of *Setd1a* (+/−) mice.

(D) Band signals (left) and the amount of SETD1A protein by western blotting (right) in *Setd1a* (+/+) and *Setd1a* (+/−) mice (n = 9 mice for each genotype). ***p < 0.001, Mann-Whitney *U* test. The signal intensity of *Setd1a* (+/−) mice was normalized to that of *Setd1a* (+/+) mice.

(E) Birth rates of *Setd1a* (+/−) pups (n = 159 pups/48 dams) and *Setd1a* (+/+) pups (n = 125/48) from crossing of *Setd1a* (+/−) mice with *Setd1a* (+/+) mice. *p < 0.05, Mann-Whitney *U* test. The dashed line indicates the expected birth rate.

(F) Body weights of 2-month-old *Setd1a* (+/−) (n = 31) and *Setd1a* (+/+) (n = 27) mice. n.s., no significant difference, Mann-Whitney *U* test.

(G and H) Low- (G) and high- (H, left) magnification images of the mPFCs from *Setd1a* (+/+) and *Setd1a* (+/−) mice at P24 (n = 8 images/2 mice for each; scale bar, 1 mm/100 μm), and the frequency distribution of NeuN-labeled cells (green signals) across 12 bins (60 μm/bin) from L1 to deeper layers in the PFC (H, right). p = 0.6581 (interaction), 2-way repeated-measures ANOVA (rmANOVA). PrL, prelimbic area; IL, infralimbic area; ACC, anterior cingulate cortex area.

Error bars indicate ±SEMs.

See also Table S2 for statistics.

the stay time in the light box was also identical between genotypes (Figures 2P). Because *Setd1a* (+/−) mice showed severe immobility in the water maze, we failed to examine spatial working memory in the Morris water maze (Figures S1D–S1G), also suggesting impaired avoidance from aversive situations. In contrast, in the fear conditioning test, there were no significant differences in freezing levels in both context and cue tasks (Figure S1H), indicating intact fear memory and learning in *Setd1a* (+/−) mice.

These behavioral results collectively indicate that *Setd1a* (+/−) mice exhibit multiple abnormal behaviors relevant to SCZ.

Excitatory Synaptic Function in L2/3 Pyramidal Neurons of the mPFC Is Attenuated in *Setd1a* (+/−) Mice

To assess whether the reduction of SETD1A impairs synaptic function in the mPFC, we performed whole-cell recording from L2/3 pyramidal neurons of the mPFC of *Setd1a* (+/−) mice at postnatal day 18 (P18) to P25 (Figure 3A). We found that both the frequency and the amplitude of the spontaneous excitatory postsynaptic current (sEPSC) were significantly reduced (Figures 3B and 3C), whereas either parameter of the spontaneous inhibitory postsynaptic current (sIPSC) was not changed (Figures S2A and S2B), in *Setd1a* (+/−) mice. We then analyzed quantal synaptic responses by recording miniature EPSC (mEPSC) and mIPSC and found a significant reduction in the frequency but not the amplitude of mEPSC in *Setd1a* (+/−) neurons (Figures 3D and 3E). Consistent with the results of sIPSC, no significant difference was found in either the frequency or the amplitude of mIPSC (Figures S2C and S2D). Then, we recorded EPSCs evoked by local electrical stimulation in L2/3 of the mPFC. We found that both α-amino-3-hydroxy-5-methyl-4-isoxazolepropionic acid

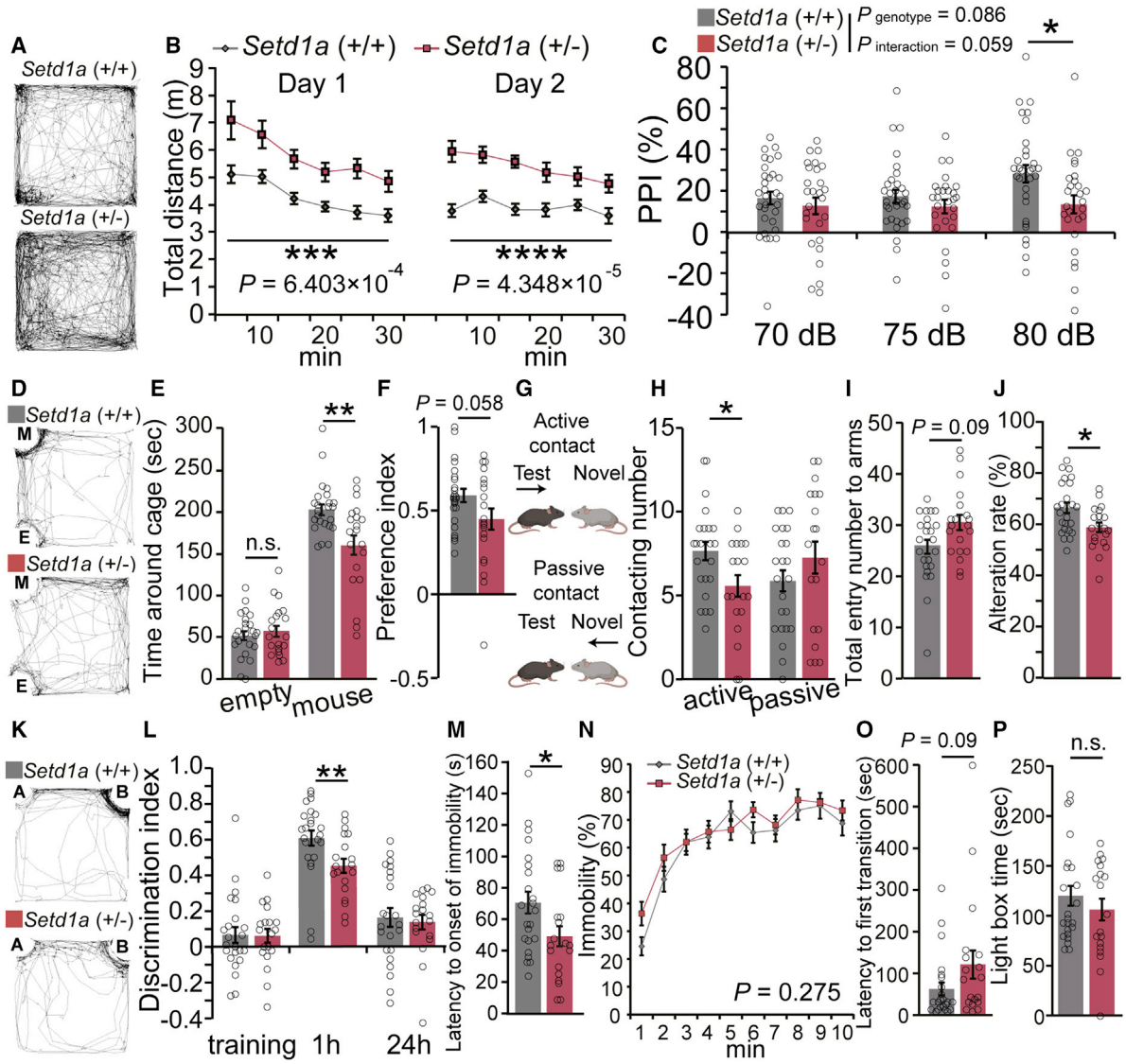

Figure 2. *Setd1a* (+/−) Mice Display Multiple Behavioral Abnormalities Relevant to SCZ

(A and B) Open field tests. Representative tracks (A) and the total distances traveled (B) in each trial day for *Setd1a* (+/−) (n = 20) and *Setd1a* (+/+) (n = 24) mice. ***p < 0.001, ****p < 0.0001 (genotype), 2-way rmANOVA.

(C) Prepulse inhibition test. Inhibition of startle response to 120 dB sound following prepulse of 70, 75, and 80 dB for *Setd1a* (+/+) (n = 31) and *Setd1a* (+/−) (n = 27) mice. p = 0.086 (genotype) and p = 0.0591 (interaction), 2-way rmANOVA. *p < 0.05 at 80 dB prepulse, Bonferroni's post hoc multiple comparison test.

(D–F) Sociality test. Representative tracks of social interaction in the arena (D), the spent time around the empty and mouse cages (E), and the preference index (F) for *Setd1a* (+/−) (n = 20) and *Setd1a* (+/+) (n = 24) mice. n.s., not significant and **p < 0.01, Mann-Whitney *U* test (E). p = 0.058, Student's t test (F).

(G and H) Reciprocal social interaction test. Experimental schemes (G) and the number of active and passive contacts (H) for *Setd1a* (+/−) (n = 19) and *Setd1a* (+/+) (n = 23) mice. *p < 0.05, Mann-Whitney *U* test.

(I and J) Y-maze spontaneous alteration test. The total number of entry into the 3 arms (I) and the alteration rate of entry into arms different from the previous arm (J) for *Setd1a* (+/−) (n = 20) and *Setd1a* (+/+) (n = 24) mice. p = 0.09, *p < 0.05, Mann-Whitney *U* test.

(K and L) Novel object recognition test. Representative tracks at 1 h after the training (K) and the discrimination index of novel object (L) for *Setd1a* (+/−) (n = 19) and *Setd1a* (+/+) (n = 24) mice. **p < 0.01, Mann-Whitney *U* test.

(M and N) Tail suspension test. The latency to onset (M) and the percentage of immobility (N) for *Setd1a* (+/−) (n = 20) and *Setd1a* (+/+) (n = 24) mice. *p < 0.05 for (M), p = 0.275 (genotype) for (N).

(O and P) Light/dark transfer test. The latency to the first transition from dark to light box (O) and the time spent in the light box (P) for *Setd1a* (+/−) (n = 20) and *Setd1a* (+/+) (n = 24) mice. p = 0.09, n.s., Mann-Whitney *U* test.

Error bars indicate ±SEMs.

See also Figure S1 and Table S2.

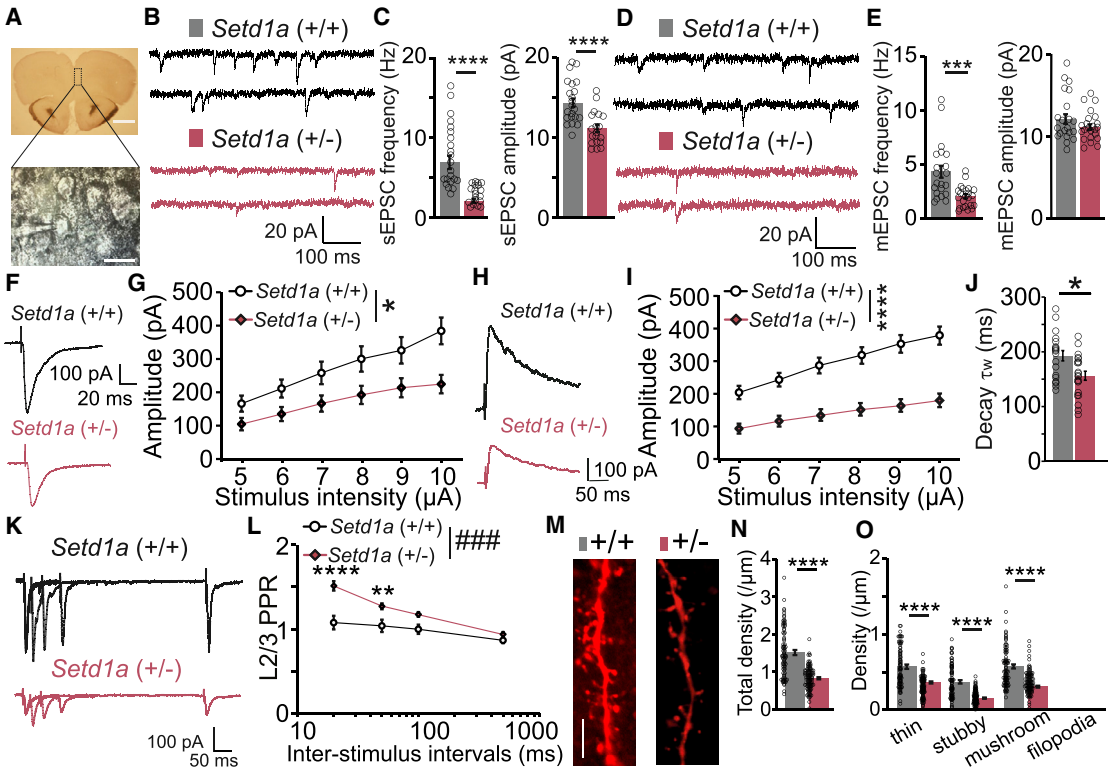

Figure 3. Attenuated Excitatory Synaptic Function and Structure in L2/3 Pyramidal Neurons of the mPFCs of *Setd1a* (+/−) Mice

(A) Images of an acute coronal slice (top) and L2/3 pyramidal neurons of the mPFC during whole-cell recording (bottom). Scale bar, 1 mm/50 μm.

(B and C) Sample traces (B) and the average frequency and amplitude of sEPSCs (C) from *Setd1a* (+/+) (n = 22 cells/3 mice) and *Setd1a* (+/−) (n = 19/3) neurons. ****p < 0.0001, Mann-Whitney *U* test.

(D and E) Sample traces (D) and the average frequency and amplitude of mEPSCs (E) from *Setd1a* (+/+) (n = 21/3) and *Setd1a* (+/−) (n = 23/3) neurons. ***p < 0.001, Mann-Whitney *U* test.

(F and G) Sample traces (F) and the average amplitude of AMPAR-mediated eEPSCs by local L2/3 stimulation from *Setd1a* (+/+) (n = 24/3) and *Setd1a* (+/−) (n = 24/3) neurons. *p < 0.05 (genotype), 2-way rmANOVA.

(H–J) Sample traces (H), the average amplitude (I), and decay kinetics (weighted tau [τ_w]) (J) of NMDAR-mediated eEPSCs from *Setd1a* (+/+) (n = 24/3) and *Setd1a* (+/−) (n = 24/3) neurons. ****p < 0.0001 (genotype), 2-way rmANOVA (I). *p < 0.05, Mann-Whitney *U* test (J).

(K and L) Sample traces (K) and the average PPR of eEPSCs e at 20, 50, 100, and 500 ms interstimulus intervals from *Setd1a* (+/+) (n = 24/3) and *Setd1a* (+/−) (n = 23/3) mice. $^{\#\#\#}$p < 0.001 (genotype), 2-way rmANOVA. **p < 0.01 and ****p < 0.0001, Bonferroni's post hoc multiple comparison test.

(M–O) Sample images (M, scale bar, 5 μm) and the density (N) and classification (O) of dendritic spines for *Setd1a* (+/−) (n = 85 dendrites/2 mice) and *Setd1a* (+/+) (n = 105/2) neurons. ****p < 0.0001, Mann-Whitney *U* test.

Error bars indicate ±SEMs.

See also Figure S2 and Table S2.

(AMPAR)-mediated (Figures 3F and 3G) and *N*-methyl-D-aspartate receptor (NMDAR)-mediated (Figures 3H and 3I) evoked EPSCs (eEPSCs) were significantly reduced in amplitude in *Setd1a* (+/−) neurons (Figures 3F–3I). Moreover, the kinetics of NMDAR-mediated eEPSCs were faster in *Setd1a* (+/−) neurons (Figure 3J), suggesting the possibility of altered NMDAR subunit composition (Bellone and Nicoll, 2007; Paoletti et al., 2013).

The reduced frequency of mEPSC indicates the reduced number of functional excitatory synapses and/or the reduced release probability of glutamate from presynaptic terminals. To evaluate release probability, we applied paired stimulation and measured paired-pulse ratio (PPR) (Figures 3K and 3L). PPR was significantly increased in *Setd1a* (+/−) neurons (Figure 3L), indicating a reduced release probability. To assess possible postsynaptic changes, we examined spine density (Figure 3M) and found that the total density was significantly lower in *Setd1a* (+/−) mice than in *Setd1a* (+/+) mice (Figure 3N). Notably, thin, stubby, and mushroom-type spines were reduced in density (Figure 3O). While excitatory synaptic inputs were reduced in *Setd1a* (+/−) neurons, parameters for intrinsic excitability, including the frequency of spikes in response to depolarization, rheobase, resting membrane potential, and input resistance, were not different between genotypes (Figures S2E–S2I).

These data indicate that excitatory synaptic transmission in L2/3 pyramidal neurons was attenuated in *Setd1a* (+/−) neurons by affecting both presynaptic and postsynaptic components, which induces an imbalance of excitation and inhibition of L2/3 neurons of the mPFC.

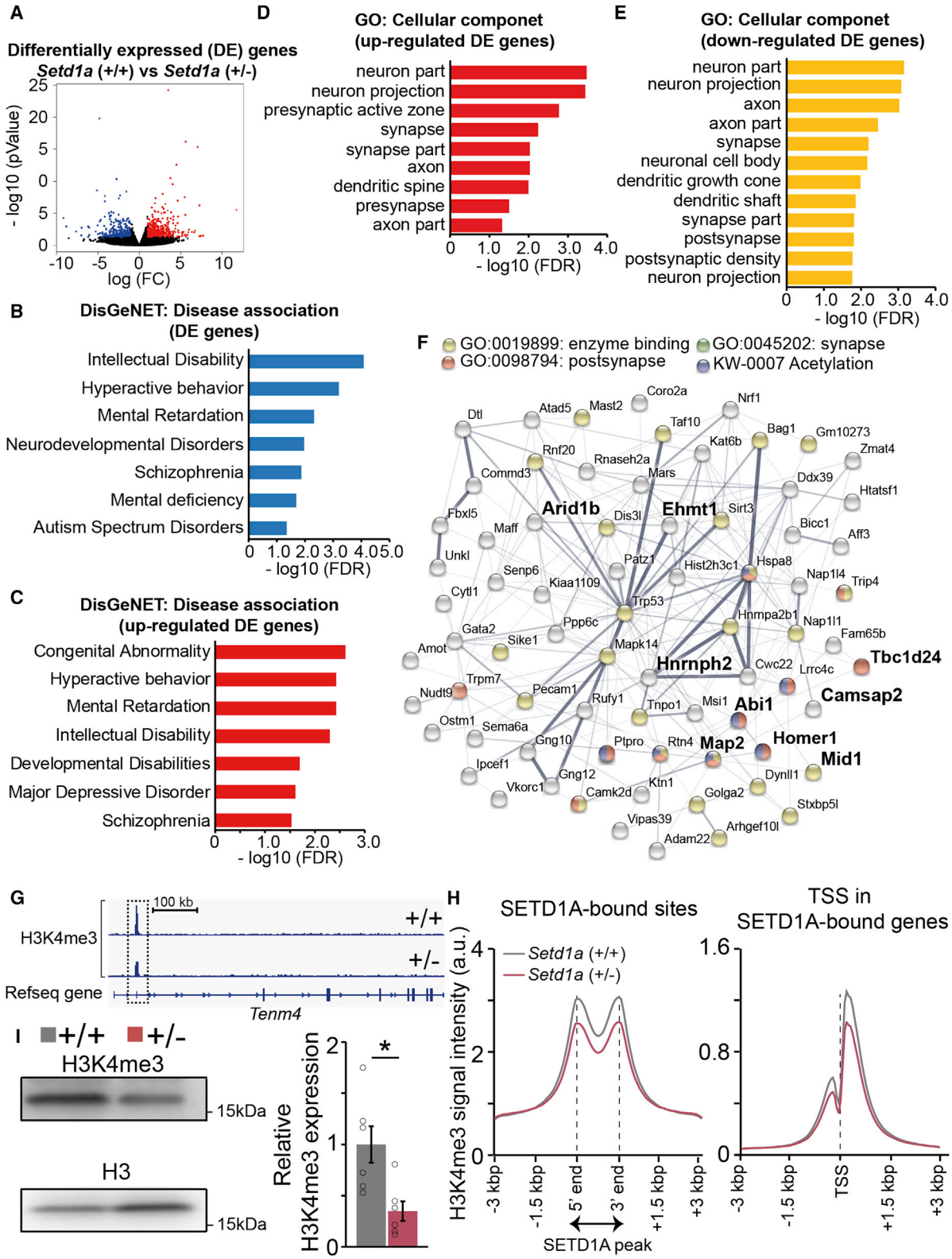

(legend on next page)

Altered Expression of Genes Associated with Neurodevelopmental Disorders (NDDs) in *Setd1a* (+/−) Mice

Epigenomic enzymes such as SETD1A regulate the diverse expression of their target genes through their catalytic activities of histone modification (Greer and Shi, 2012). To evaluate how expression patterns of transcriptomes in *Setd1a* (+/−) mice are altered, we performed RNA-seq on the samples of whole mPFC tissues dissected from *Setd1a* (+/+) and *Setd1a* (+/−) mice. We quantified differentially expressed (DE) genes and found that 547 genes were downregulated and 878 genes were upregulated in *Setd1a* (+/−) mice compared to *Setd1a* (+/+) mice (Figure 4A). Among these genes, 9 downregulated genes and 3 upregulated genes overlapped between the transcriptomes of our RNA-seq data and the previous data by Mukai et al. (2019) (Figure S3). We analyzed how DE genes were related to SCZ and other NDDs such as autism spectrum disorder (ASD) and intellectual disability (ID). We performed a disease-enrichment analysis, showing a significant enrichment for ID, NDDs, SCZ, and ASD terms (Figure 4B), which is consistent with the identification of *SETD1A* mutations in other NDDs in a previous whole-exome sequencing study (Singh et al., 2016). Furthermore, the DE genes in *Setd1a* (+/−) mice were also related to "hyperactive behavior" (Figure 4B), which is consistent with our behavioral results (Figures 2A and 2B). We then analyzed the disease terms of the up- and downregulated DE genes and found that the upregulated genes were enriched in the terms related to developmental abnormality such as "congenital abnormality," "mental retardation," and ID (Figure 4C). In contrast, the downregulated genes did not display any significant enrichment in the disease annotations. Because H3K4me3 by SETD1A enhances the targeted gene expression, the results suggest that NDD-related genes are likely to be regulated by SETD1A indirectly. Based on these analyses, we speculate that SETD1A regulates multiple molecular cascades involved in not only SCZ but also other NDDs.

Altered Expression of Genes Related to Presynaptic and Postsynaptic Functions in *Setd1a* (+/−) Mice

Next, we investigated to which biological function the up- and downregulated DE genes in *Setd1a* (+/−) mice are related by Gene Ontology (GO) analysis using the STRING online program. We found that the upregulated DE genes were enriched in the annotations of not only postsynaptic but also presynaptic function such as "presynaptic active zone," "presynapse," and "dendritic spine" (Figure 4D). In contrast, the downregulated DE genes enriched in the annotations more preferentially of postsynaptic functions such as "postsynapse" and "postsynaptic density" (Figure 4E), which is consistent with our electrophysiological and spine morphological data in the mPFC (Figure 3). In addition, the downregulated DE genes included those related to epigenomic functions such as acetylation (Figure 4F). These proteins are supposed to interact with one another based on the protein-protein interaction analysis performed by the STRING program (Figure 4F). To examine whether the epigenomic state was affected in the mPFC of *Setd1a* (+/−) mice, we conducted chromatin immunoprecipitation sequencing (ChIP-seq) on PFC samples from *Setd1a* (+/−) and *Setd1a* (+/+) mice to check the H3K4me3 levels at specific gene loci (Figures 4G and 4H) around the SETD1A-bound sites reported previously (Mukai et al., 2019). In their ChIP-seq using the anti-SETD1A antibody, Mukai et al. (2019) examined transcriptional start sites (TSSs) in the gene loci with SETD1A-bound sites, including the *Tenm4* locus. According to their scRNA-seq data, the *Tenm4* locus was specifically expressed in a cluster of pyramidal neurons of the mPFC (Mukai et al., 2019). Based on the previous data, our own ChIP-seq showed that the signal intensity of H3K4me3 in both SETD1A-bound sites and TSSs in SETD1A-bound genes was decreased in *Setd1a* (+/−) mice (Figures 4G and 4H). Furthermore, we performed western blotting of PFC samples with an antibody-recognizing tri-methylated lysine 4 of histone H3 and found that the H3K4me3 band signal was decreased in *Setd1a* (+/−) mice compared to *Setd1a* (+/+) mice (Figure 4I). These results suggest that the reduction of SETD1A changes the expression of many genes related to presynaptic and postsynaptic functions, presumably by reducing the H3K4me3 level.

Deletion of *Setd1a* Impairs Both Presynaptic and Postsynaptic Functions in L2/3 Pyramidal Neurons of the mPFC

To further investigate the roles of *Setd1a* in synaptic transmission, we performed RNAi-mediated *Setd1a* KD in L2/3 pyramidal neurons of the mPFC by *in utero* electroporation (IUE) at E14.5.

Figure 4. Expected Functions of Differentially Expressed (DE) Genes between *Setd1a* (+/−) and *Setd1a* (+/+) Mice

(A) Volcano plot showing DE genes in the mPFC between *Setd1a* (+/−) and *Setd1a* (+/+) mice at P30 (n = 3 for each genotype). Blue and red dots indicate 547 downregulated and 878 upregulated genes, respectively.

(B and C) Disease terms of DisGeNET database associated with the DE genes (B) and with the upregulated DE genes (C) in *Setd1a* (+/−) mice. The disease terms were not associated with the downregulated DE genes.

(D and E) GO annotations related to neuronal functions associated with the upregulated (D) and the downregulated (E) DE genes in *Setd1a* (+/−) mice.

(F) Diagram for downregulated protein network showing the interactions between synaptic functions and epigenomic modifications such as acetylation. Bold characters indicate neurodevelopmental disorder (NDD)-related genes.

(G and H) Representative ChIP-seq data in *Tenm4* locus (G) and histogram of H3K4me3 signal intensity around SETD1A-bound DNA regions (H, left) and that around transcriptional start sites (TSSs) of SETD1A-bound genes (H, right) reported in Mukai et al. (2019) from P30 age-matched *Setd1a* (+/+) mice (n = 3) and *Setd1a* (+/−) mice (n = 4). The box with the dashed line in (G) indicates H3K4me3 signal peaks in *Tenm4* locus from the 2 genotypes. The H3K4me3 signal intensity was normalized by spike-in genome of HEK293T cells. a.u., arbitrary unit.

(I) Band signals (left) and H3K4me3 levels (6 mice for each genotype). $p < 0.05$, Mann-Whitney *U* test. The signal intensity of *Setd1a* (+/−) mice was normalized to that of *Setd1a* (+/+) mice. Error bars indicate ±SEMs.

(B–E) False discovery rate (FDR) < 0.05 and $p < 0.05$ between genotypes; Benjamini and Hochberg's method.

See also Figure S3 and Table S2.

We constructed microRNAs (miRNAs) against two different regions of the *Setd1a* sequence, and validated their effects and specificities *in vitro* and *in vivo* (Figures S4A–S4D). We estimated that ~30% of Ca^{2+}/calmodulin-dependent protein kinase II-positive ($CaMKII^{+}$) pyramidal neurons were transfected with the *Setd1a*-KD vectors in the mPFC that underwent IUE (Figures S4E and S4F). We prepared coronal slices, including the mPFC from mice at P16–P25, and performed whole-cell recordings from GFP^{+} *Setd1a*-KD neurons and GFP^{-} control neurons in the prelimbic and infralimbic regions of the mPFC (Figures 5A and 5B). We found that both the frequency and the amplitude of mEPSC were significantly smaller in *Setd1a*-KD neurons than in control neurons (Figures 5C and 5D), which was similar but more severe than the phenotypes seen in *Setd1a* (+/−) mice (Figures 3D and 3E). The effects of *Setd1a* KD on mEPSCs were fully restored when the *Setd1a*-rescue vector was co-expressed, which excluded off-target effects of the used miRNAs (Figures 5C and 5D). The results indicate that KD of *Setd1a* in L2/3 pyramidal neurons of the mPFC also attenuated excitatory synaptic transmission. We then recorded AMPAR- and NMDAR-mediated eEPSCs in response to local electrical stimulation in L2/3. We found that *Setd1a*-KD neurons had significantly smaller amplitudes of AMPAR- and NMDAR-mediated eEPSCs (Figures 5E–5H) and increased PPRs (Figures 5I and 5J) than control neurons. These results were fully consistent with those of *Setd1a* (+/−) mice (Figures 3F–3K). Next, to examine the spine density of *Setd1a*-KD neurons, we sparsely labeled a subset of L2/3 pyramidal neurons with mOrange, among those expressing *Setd1a*-Scr or *Setd1a*-KD miRNA together with GFP (Figure S4G). We found that the total spine density and the density of thin and mushroom-type spines were significantly reduced in *Setd1a*-KD neurons compared to *Setd1a*-Scr neurons (Figures 5K–5M). These results were essentially similar to those of the *Setd1a* (+/−) neurons (Figures 3L–3O). Although inhibitory synaptic transmission was not impaired in *Setd1a* (+/−) neurons (Figures S2A–S2D), the frequency of mIPSCs (Figures 5N and 5O) and the amplitude of evoked IPSCs (Figures 5P and 5Q) were reduced in the *Setd1a*-KD neurons, indicating that inhibitory synaptic transmission was attenuated in *Setd1a*-KD neurons.

Deletion of *Setd1a* in Postsynaptic Neurons Reduces Glutamate Release Probability

We further investigated whether the loss of *Setd1a* in the presynaptic neuron and/or in the postsynaptic neuron was responsible for the attenuation of eEPSCs. To tackle this issue, we recorded from *Setd1a*-KD and control neurons in L2/3 of the same slices and stimulated in L5, where neurons and nerve fibers showed no GFP signals and therefore were not transfected with *Setd1a*-KD miRNAs (Figure 6A). We found that the amplitude of eEPSCs was significantly smaller and the PPR was significantly larger in *Setd1a*-KD neurons than in control neurons in L2/3 (Figures 6B and 6C), indicating that *Setd1a* KD in postsynaptic neurons causes the reduction in eEPSC amplitude and the elevation of PPR.

To examine the effects of *Setd1a* KD in presynaptic neurons, we transfected a vector for channelrhodopsin-2 (ChR2) expression together with a vector for *Setd1a*-KD and GFP expression or with that for *Setd1a*-Scr and GFP expression in L2/3 neurons of the mPFCs of different mice by means of IUE (Figure 6D). We recorded from untransfected control neurons and stimulated presynaptic *Setd1a*-Scr or *Setd1a*-KD neurons by light pulses (Figure 6D). The strength of light was adjusted to generate optic EPSCs with an amplitude of ~50–100 pA. We found that the PPR was similar between the *Setd1a*-Scr and the *Setd1a*-KD groups (Figures 6E and 6F), indicating that *Setd1a* KD in presynaptic neurons had no effect on PPR.

Then, to test the effect of *Setd1a* KD in both presynaptic and postsynaptic neurons, we sparsely expressed the highly light-sensitive opsin Chronos together with GFP in a Cre-dependent manner in L2/3 pyramidal neurons that expressed *Setd1a*-KD miRNAs together with mOrange (see Method Details). We stimulated *Setd1a*-KD neurons expressing Chronos and GFP by light pulses and recorded EPSCs from control neurons and *Setd1a*-KD neurons expressing mOrange in the same slices (Figure 6G). We found that the amplitude of evoked EPSCs was significantly smaller and the PPR was significantly larger in *Setd1a*-KD neurons than in control neurons (Figures 6H and 6I), indicating that the reduction in eEPSC amplitude and the elevation of the PPR resulted from the lack of *Setd1a* in postsynaptic neurons. We confirmed that optogenetically induced EPSCs in L2/3 pyramidal neurons were monosynaptic for the following reasons. The responses evoked by light stimulation of ChR2-expressing neurons were totally abolished by tetrodotoxin (TTX; 1 μM), and the responses were fully recovered when light-evoked depolarization of presynaptic neurons was enhanced by adding 4-aminopyridine (4-AP; 1 mM) (Figure S5A). Furthermore, the latency and jitter of optogenetically induced EPSCs were identical between EPSCs elicited from ChR2-expressing *Setd1a*-Scr neurons and those from ChR2-expressing *Setd1a*-KD neurons (Figure S5B) or between EPSCs elicited from Chronos-expressing *Setd1a*-KD neurons in control neurons and those in *Setd1a*-KD neurons (Figure S5C).

Our RNA-seq analysis indicates that a number of genes encoding presynaptic and postsynaptic proteins are differentially expressed in the mPFC between *Setd1a* (+/+) and *Setd1a* (+/−) mice (Figures 4D–4F). We therefore performed quantitative reverse transcription-PCR (qRT-PCR) analysis of GFP^{+} regions of mPFC tissues from *Setd1a*-Scr and *Setd1a*-KD mice to examine quantitatively the level of expression of such genes (Figure S4C). We found that two representative postsynaptically expressed genes, *Homer1* and *Ptpro*, exhibited significant reductions, whereas a representative presynaptically expressed gene, *Unc13c*, showed no change in *Setd1a*-KD mice (Figure 6J).

The results of the 3 sets of electrophysiological experiments (Figures 6A–6I) and the significant reduction in gene expression for postsynaptic proteins (Figure 6J) indicate that the loss of *Setd1a* in postsynaptic L2/3 pyramidal neurons but not in presynaptic neurons causes the reduction in neurotransmitter release probability in presynaptic neurons.

Elevated Inhibition/Excitation (I/E) Balance of Synaptic Inputs in *Setd1a*-KD Neurons

In L2/3 pyramidal neurons of the mPFC of *Setd1a* (+/−) mice, excitatory synaptic transmission was attenuated, but inhibitory

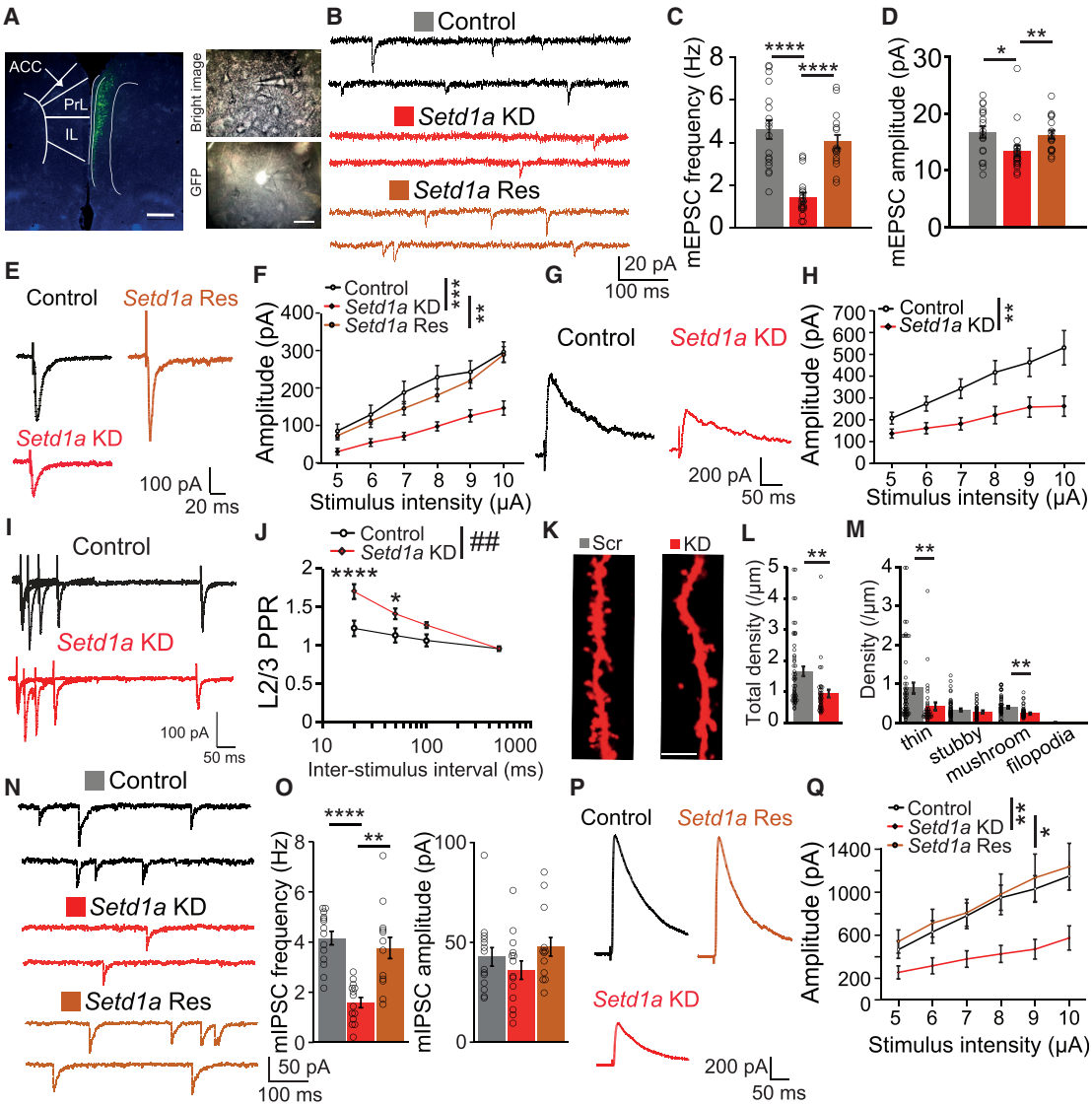

Figure 5. *Setd1a* KD in L2/3 Pyramidal Neurons of the PFC Attenuates Excitatory Synaptic Function and Structure

(A) Low-magnification image of a coronal brain slice with GFP signals in the mPFC (left) and high-magnification images of a brain slice during recording (right). Scale bar, 1 mm/50 μm.

(B–D) Representative traces (B) and the average frequency (C) and amplitude (D) of mEPSCs from control (n = 18/5), *Setd1*-KD (n = 19/5), and *Setd1a*-rescue (*Setd1a*-Res) (n = 16/3) neurons. *p < 0.05, **p < 0.01, ****p < 0.0001, Kruskal-Wallis test with Steel-Dwass post hoc analysis.

(E and F) Sample traces (E) and the average AMPAR-mediated eEPSC amplitude (F) from control (n = 13/4), *Setd1a*-KD (n = 13/4), and *Setd1a*-Res (n = 19/3) neurons. **p < 0.01 (treatment), ***p < 0.001 (treatment), 2-way rmANOVA.

(G and H) Sample traces (G) and the average amplitude (H) of NMDAR-mediated eEPSC from control (n = 17/5) and *Setd1a*-KD (n = 18/5) neurons. **p < 0.01 (treatment), 2-way rmANOVA.

(I and J) Sample traces (I) and the average PPR (J) of eEPSCs for control (n = 16/5) and *Setd1a*-KD (n = 16/5) neurons. $^{\#\#}$p < 0.01 (treatment), 2-way rmANOVA. *p < 0.05, ****p < 0.0001, Bonferroni's post hoc multiple comparison test.

(K–M) Sample images (K, scale bar, 5 μm), the density (L), and classification (M) of spines for *Setd1a*-Scr (n = 51 dendrites/3 mice) and *Setd1a*-KD (n = 36/3) neurons. **p < 0.01, Mann-Whitney *U* test.

(N and O) Sample traces (N) and the average frequency and amplitude (O) of mIPSC from control (n = 14/3), *Setd1a*-KD (n = 14/3), and *Setd1a*-Res (n = 12/3) neurons. **p < 0.01, ****p < 0.0001, Kruskal-Wallis test with Steel-Dwass post hoc analysis.

(P and Q) Sample traces (P) and the average amplitude of evoked IPSCs (Q) from control (n = 13/3), *Setd1a*-KD (n = 13/3), and *Setd1a*-Res (n = 12/3) neurons. *p < 0.05 (treatment), **p < 0.01 (treatment), 2-way rmANOVA.

Error bars indicate ±SEMs.

See also Figure S4 and Table S2.

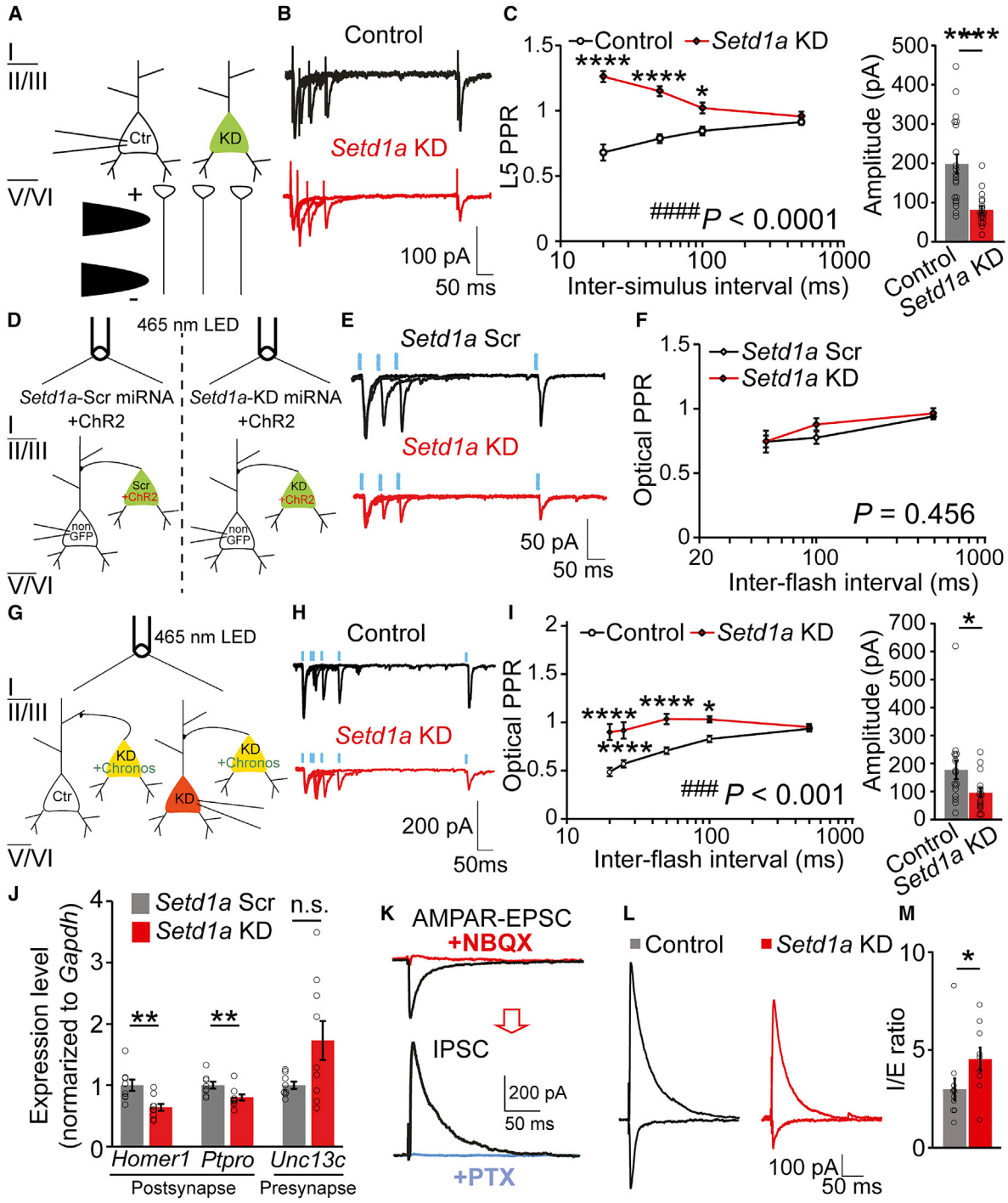

Figure 6. Deletion of *Setd1a* in Postsynaptic L2/3 Pyramidal Neurons Reduces Glutamate Release Probability and Elevates Inhibition/Excitation (I/E) Balance

(A–C) Experimental scheme (A), sample traces (B), and the average PPR (C, left) and the average amplitudes (C, right) of EPSCs from control (n = 20/4), and *Setd1a*-KD (n = 19/4) neurons induced by electrical stimulation (8 μA) in L5 of the same slices. $^{####}p < 0.0001$ (treatment), 2-way rmANOVA. *p < 0.05, ****p < 0.0001, Bonferroni's post hoc multiple comparison test for PPR and Mann-Whitney *U* test for amplitude.

(D–F) Experimental scheme (D), sample traces (E), and the average PPR (F) of EPSCs recorded from GFP^- neurons by optically activating presynaptic neurons expressing ChR2 with the *Setd1a*-Scr vector (Scr+ChR2, n = 15/3) or those expressing ChR2 with the *Setd1a*-KD vector (KD+ChR2, n = 22/4) in different mice. p = 0.456 (treatment), 2-way rmANOVA.

(legend continued on next page)

synaptic transmission was normal (Figures 3 and S2A–S2D). By contrast, L2/3 pyramidal neurons with *Setd1a* KD were impaired in both excitatory and inhibitory synaptic functions (Figure 5). To assess the net effect of *Setd1a* KD on synaptic inputs to L2/3 pyramidal neurons, we examined the ratio of excitatory and inhibitory synaptic inputs in individual neurons (Rothwell et al., 2014). We stimulated locally in L2/3 and recorded AMPAR-mediated eEPSCs and evoked IPSCs at holding potentials of −40 and 0 mV, respectively. The 2 types of synaptic responses were validated pharmacologically by the AMPAR antagonist 2,3-dioxo-6-nitro-7-sulfamoyl-benzo[f]quinoxaline (NBQX; 10 μM) or the $GABA_A$ receptor (GABAR) blocker picrotoxin (100 μM) under the blockade of NMDARs with AP-5 (50 μM) (Figure 6K). We found that the ratio of the amplitude of evoked IPSC over that of AMPAR-mediated eEPSC was significantly larger in *Setd1a*-KD neurons than in control neurons (Figures 6L and 6M), indicating that *Setd1a* deletion elevated the I/E balance in L2/3 pyramidal neurons of the mPFC.

Setd1a KD in L2/3 Pyramidal Neurons of the Bilateral PFC Impairs Social Behavior

To assay the outcome of *Setd1a* deletion in L2/3 pyramidal neurons of the PFC on mouse behavior, we knocked down *Setd1a* widely from the bilateral frontal cortex including the mPFC (bilateral *Setd1a*-KD mice) by IUE with the triple-electrode probe (dal Maschio et al., 2012; Szczurkowska et al., 2016) (Figure S6A). We quantified the area of GFP expression reflecting transfected L2/3 pyramidal neurons in coronal brain slices from bilateral *Setd1a*-Scr/KD mice (Figures S6B–S6E). We confirmed that GFP^+ areas were mainly located in the mPFC, the dorsolateral PFC (DLPFC), and the cingulate cortex (cgCx) (Figures S6D and S6E). Then, we performed the behavioral tests on bilateral *Setd1a*-Scr/KD mice as we did on *Setd1a* (+/−) mice (Figure 7). In contrast to *Setd1a* (+/−) mice, locomotor activity in the open field test (Figure 7A) and the performance in the prepulse inhibition test (Figure 7B) were not altered in *Setd1a*-KD mice when compared to *Setd1a*-Scr mice. However, in the sociality test, the spent time around the novel mouse cage and the preference index were both decreased significantly in *Setd1a*-KD mice (Figures 7C–7E), which is consistent with the behavioral phenotype of *Setd1a* (+/−) mice. As for the other behavioral tests, *Setd1a*-KD mice exhibited a normal alteration rate in the Y-maze spontaneous alteration test (Figure 7F), unimpaired short-term cognitive memory in the object recognition test (Figure 7G), and normal avoidance behaviors in the tail suspension test and the light/dark transfer test (Figures 7H–7K). These results suggest that *Setd1a* KD in L2/3 pyramidal neurons of the bilateral frontal cortex specifically affects sociality in mice.

DISCUSSION

Our *Setd1a* (+/−) mice had attenuated excitatory synaptic transmission in L2/3 pyramidal neurons of the mPFC and displayed various abnormal behaviors that are relevant to symptoms of SCZ, including hyperactivity, impaired sociality, and deficit in working memory. Some of these phenotypes were not seen in the $Setd1a^{+/-}$ mice recently reported by Mukai et al. (2019) (Table S1). What would be the reasons for the differences? The first possibility would be the difference in the way that *Setd1a* knockout mice are generated. Our *Setd1a* (+/−) mice were generated with the CRISPR-Cas9 system by inducing a 2-base deletion to cause a frameshift mutation in exon 7 of the *Setd1a* gene body. It is theoretically possible that the CRISPR-Cas9 system exerted off-target effects against other genes. However, we used the following strategies to minimize the possible off-target effects. First, we chose one unique single-guide RNA (sgRNA) from 5 candidates whose sequence was not homologous to the other genes for 20 bases upstream of protospacer adjacent motif by the online program (also see STAR Methods). Second, our *Setd1a* (+/−) mice were backcrossed to wild-type C57B6/N strain >3 times to reduce the likelihood of any off-target mutations. Third, in each analysis, we compared *Setd1a* (+/−) mice with *Setd1a* (+/+) mice in the same litters to normalize the genomic factors, except the *Setd1a* mutation.

Mukai et al. (2019) used, in contrast to our *Setd1a* (+/−) mice, the transgenic mouse line carrying the insertion of the LacZ/Neo cassette in the upstream of exon 4 (Bledau et al., 2014). Several reports show that the phenotypes of transgenic mice of a certain gene could vary depending on the site and/or type of mutation of that gene. For example, transgenic mice with a single guanine nucleotide (G) insertion at *Shank3* to induce a frameshift mutation seen in ASD patients (InsG3680 mutation) displayed increased mEPSC amplitude in striatal medium spiny neurons, impaired social interaction, and strong repetitive/compulsive grooming behaviors, whereas mice carrying a point mutation to change arginine (R) to a stop codon identified in SCZ patients (R1117X mutation) did not show these phenotypes (Zhou et al., 2016). Furthermore, mouse lines carrying different types of missense mutation resulting in amino acid change (Q31L and L100P) in the *Disc1* gene showed different behavioral phenotypes in social novelty preference and forced swim immobility (Clapcote et al., 2007). These lines of evidence suggest that different types and positions of mutation in the same gene may cause different phenotypes of behaviors and synaptic properties in mice.

There are several other possibilities that may have caused the phenotypic differences between our *Setd1a* (+/−) mice and the

(G–I) Experimental scheme (G), sample traces (H), and the average PPR (I, left) and average amplitudes (I, right) of EPSCs evoked by optical stimulation of Chronos-expressing and *Setd1a*-KD presynaptic neurons and recorded from control (n = 16/6) and *Setd1a*-KD (n = 15/6) neurons in the same slices. $^{\#\#\#}p < 0.001$ (treatment), 2-way rmANOVA. $^*p < 0.05$ and $^{****}p < 0.0001$, Bonferroni's post hoc multiple comparison test for PPR and Mann-Whitney *U* test for amplitude.
(J) Quantitative reverse transcription-PCR (qRT-PCR) for the expression levels of representative genes encoding postsynaptic proteins (*Homer1* and *Ptpro*) and a presynaptic protein (*Unc13c*) in GFP^+ areas of mPFC slices from *Setd1a*-Scr (n = 8) and *Setd1a*-KD mice (n = 9). Note that these three genes were identified to be downregulated in the mPFCs of *Setd1a* (+/−) mice (Figure 4F). n.s. and $^{**}p < 0.01$, Mann-Whitney *U* test.
(K–M) Diagram of experimental procedures (K), sample traces of inhibitory and excitatory synaptic currents from the same pyramidal neurons (L), and the average I/E ratio (M) for control (n = 11/5) and *Setd1a*-KD (n = 9/5) neurons. $^*p < 0.05$, Mann-Whitney *U* test.
Error bars indicate ±SEMs.
See also Figure S5 and Table S2.

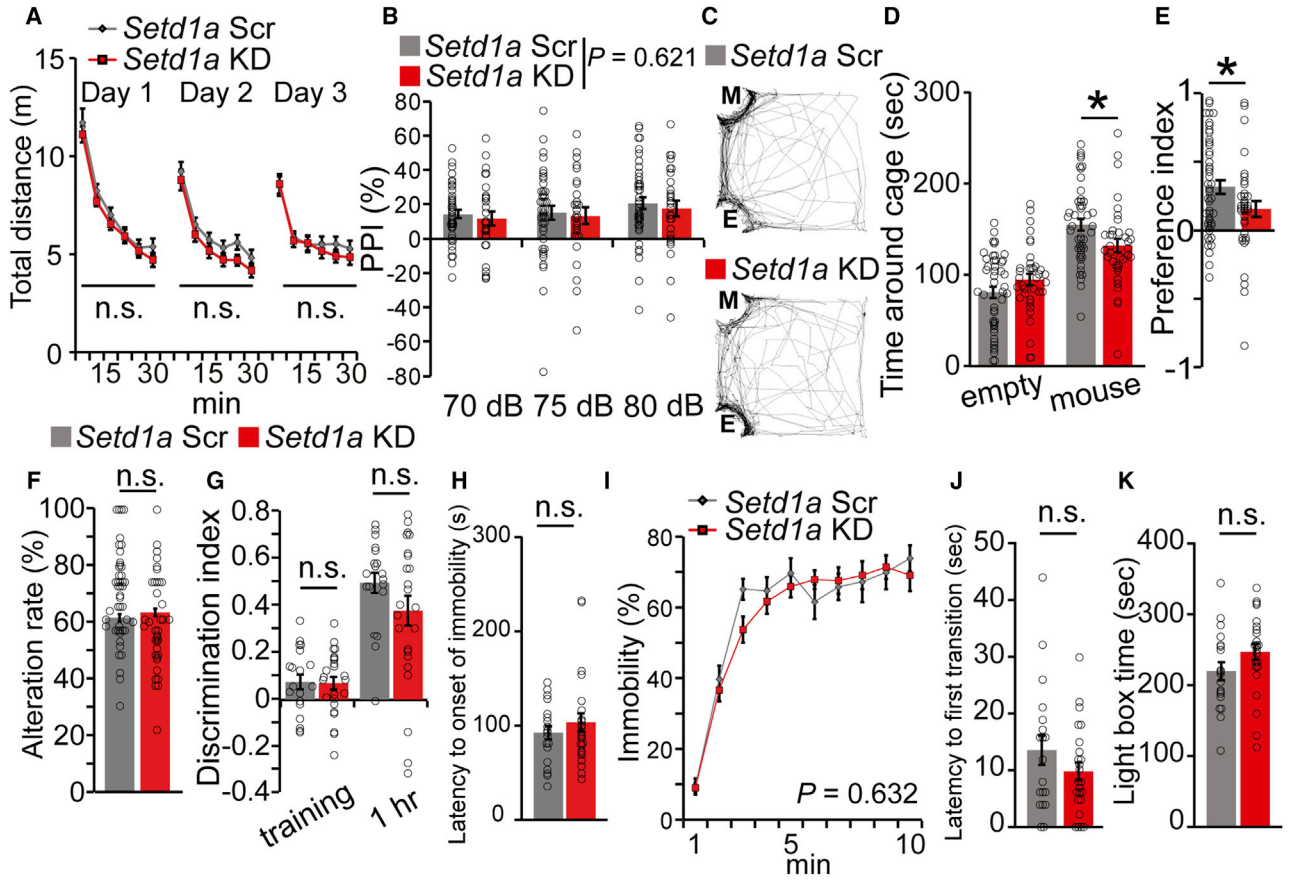

Figure 7. *Setd1a* KD in L2/3 Pyramidal Neurons of the Bilateral Frontal Cortices Impairs Social Preference in Mice

(A) Open field test. Total distance traveled in each trial day from *Setd1a*-Scr (n = 19) and *Setd1a*-KD (n = 24) mice. n.s., (treatment), 2-way rmANOVA.

(B) Prepulse inhibition test. Inhibition of startle response to 120 dB sound following prepulse of 70, 75, and 80 dB from 1-month-old *Setd1a*-Scr (n = 41) and *Setd1a*-KD (n = 28) mice. p = 0.621 (treatment), 2-way rmANOVA.

(C–E) Sociality test. Representative tracks (C), the average staying time around the empty and mouse cages (D), and the social preference index (E) for *Setd1a*-Scr (n = 46) and *Setd1a*-KD (n = 36) mice. *p < 0.05, Mann-Whitney *U* test for (D) and Student's t test for (E).

(F) Y-maze spontaneous alteration test. The alteration rate from *Setd1a*-Scr (n = 46) and *Setd1a*-KD (n = 37) mice. n.s., Mann-Whitney *U* test.

(G) Novel object recognition test. Average values of the discrimination index during and 1 h after training for *Setd1a*-Scr (n = 19) and *Setd1a*-KD (n = 24) mice. n.s., Mann-Whitney *U* test.

(H and I) Tail suspension test. The latency to onset (H) and the percentage of immobility during trials (I) for *Setd1a*-Scr (n = 19) and *Setd1a*-KD (n = 24) mice. n.s., Mann-Whitney *U* test for (H); p = 0.632 (treatment), 2-way rmANOVA for (I).

(J and K) Light/dark transfer test. The latency to first transition from dark to light box (J) and the time spent in the light box (K) for *Setd1a*-Scr (n = 19) and *Setd1a*-KD (n = 24) mice. n.s., Mann-Whitney *U* test.

Error bars indicate ±SEMs.

See also Figure S6 and Table S2.

Mukai group's *Setd1a*$^{+/-}$ mice. The first would be the difference in genetic background. Our *Setd1a* (+/−) mice were generated using the C57BL/6N mouse line, while Mukai et al. used the *Setd1a*$^{+/-}$ mice, which were backcrossed to the C57BL/6J mouse line. Previous behavioral studies reported that C57BL/6N mice showed lower activity in the open field arena, a smaller contacting number with novel mice, and a higher magnitude of PPI compared to C57BL/6J mice (Grottick et al., 2005; Matsuo et al., 2010). The second possibility would be the age of mice from which electrophysiological data were obtained. We used juvenile mice from P16 to P25, whereas Mukai et al. (2019) used 2-month-old mice to obtain electrophysiological data. The impaired excitatory synaptic transmission in L2/3 pyramidal neurons of the mPFC at the younger stage may result in various abnormal behaviors in adulthood. The third possibility would be the difference in molecular expression between the two strains of *Setd1a* mutant mice. Comparison of RNA-seq data between our *Setd1a* (+/−) mice and the Mukai et al. (2019) *Setd1a*$^{+/-}$ mice identified only a small number of commonly downregulated or upregulated genes (Figure S3). This result suggests that differences in molecular expression may underlie distinct behavioral phenotypes of the two mouse lines. The fourth possibility would be the potential differences in experimental environments that may contribute to different behaviors of mice with the same genetic backgrounds (Van Meer

and Raber, 2005). It could be possible that behavioral results in the present study and those in Mukai et al. (2019) have been spurious positive and spurious negative, respectively, because of potential subtle differences in the experimental environments. Although the exact reasons are unclear, the aforementioned factors may have influenced the phenotypic differences between our *Setd1a* (+/−) mice and the *Setd1a*$^{+/-}$ mice of Mukai et al. (2019).

We demonstrated functional and morphological attenuation of excitatory synapses in L2/3 pyramidal neurons of the mPFC of *Setd1a* (+/−) mice, including the reduced frequency of mEPSCs and the reduced densities of dendritic spines (Figures 3 and 5). We found essentially the same changes in mice with *Setd1a* KD in L2/3 pyramidal neurons of the mPFC, except that the amplitude of mEPSC was reduced in *Setd1a*-KD neurons. Since excitatory synapses are formed on dendritic spines in pyramidal neurons (Kasai et al., 2003; Spruston, 2008), the reduced mEPSC frequency and the reduced spine density indicate a reduction in the number of functional excitatory synapses in L2/3 pyramidal neurons of *Setd1a* (+/−) or *Setd1a*-KD mice. These lines of evidence strongly suggest the importance of *Setd1a* in shaping and/or maintaining postsynaptic components that are the basis for normal excitatory synaptic transmission. Our RNA-seq analysis of *Setd1a* (+/−) mice identified several downregulated genes that are believed to encode postsynaptic proteins (Figures 4E and 4F), including protein tyrosine phosphatase receptor type O (PTPRO), abelson interacting protein 1 (ABI1), and HOMER1, two of which (*Ptpro* and *Homer1*) are also decreased in the mPFC of *Setd1a*-KD mice (Figure 6J). For example, PTPRO encoded by *Ptpro* is a cell adhesion molecule that is localized to postsynaptic sites at excitatory synapses and thought to be involved in the formation of excitatory synapses. KD of *Ptpro* in cultured hippocampal neurons reduced the number of synapsin^{+} and vesicular glutamate transporter 1-positive (VGLUT1^{+}) puncta and the frequency of mEPSCs (Jiang et al., 2017). Another study reported that KD of the ABI1 gene *Abi1* reduced the number of Bassoon^{+} puncta in cultured hippocampal neurons (Proepper et al., 2007). Moreover, one of the downregulated genes, *Homer1*, encodes a scaffolding protein in postsynaptic density, and the KD of this gene was reported to decrease the spine head width in cultured hippocampal neurons (Hayashi et al., 2009). Although the previous studies for *Ptpro*, *Abi1*, and *Homer1* were performed in cultured neurons, changes in the expression of these genes may contribute to the reduced spine formation and/or maintenance in *Setd1a* (+/−) and *Setd1a*-KD neurons.

Besides postsynaptic changes, the reduction or deletion of *Setd1a* in L2/3 pyramidal neurons reduced glutamate release probability from presynaptic terminals (Figures 3K, 5J, and 6). We showed that the PPR was elevated when *Setd1a* was knocked down in the postsynaptic neuron, but not in the presynaptic neuron (Figures 6B–6I), indicating that *Setd1a* KD in postsynaptic neurons is responsible for the reduction in glutamate release from presynaptic terminals. Thus, there may be mechanisms that transmit signals from postsynaptic neurons to presynaptic terminals to maintain glutamate release probability. Several signaling molecules from postsynaptic neurons that retrogradely regulate presynaptic release probability have been identified, including the endocannabinoid 2-arachidonoylglycerol (Ohno-Shosaku and Kano, 2014; Tanimura et al., 2010), brain-derived neurotrophic factor (Poo, 2001), and nitric oxide (Hardingham and Fox, 2006). However, our RNA-seq data show no changes in the expression level of these retrograde signaling molecules (Figure 4). The identification of the factors mediating signals from postsynaptic *Setd1a*-KD neurons to presynaptic terminals awaits further studies.

Since *Setd1a* is considered to be expressed in various brain regions, it is possible that synaptic function may be altered in neurons located in brain regions other than the PFC in *Setd1a* (+/−) mice. It is also possible that the direction of change in the I/E balance may be different in different brain regions in *Setd1a* (+/−) mice. As for other genes related to neuropsychiatric disorders, several previous studies suggest that the mutation of a gene in mice caused cell-type-specific and/or brain region-specific changes in synaptic function. For example, in mice carrying a frameshift mutation of *Chd8* that is identical to that found in ASD patients, the frequency and amplitude of mIPSC were significantly altered in CA1 pyramidal neurons but not in L2/3 pyramidal neurons of the mPFC (Jung et al., 2018). In mice with *Shank3* mutations associated with ASD and SCZ, the frequency and amplitude of mEPSCs were reduced in striatal medial spiny neurons but not in pyramidal neurons of the mPFC (Zhou et al., 2016). Thus, further analyses are necessary to clarify how synaptic function is altered in brain regions other than the mPFC in *Setd1a* (+/−) mice.

Regarding the relationship between sociality and excitatory synaptic function in the mPFC as shown in our results (Figures 2, 3, 5, and 7), *Cntnap2* KO mice were reported to display impaired social behavior (Peñagarikano et al., 2011) and reduced frequency and amplitude of mEPSCs in L2/3 pyramidal neurons of the mPFC (Lazaro et al., 2019). Furthermore, a 2-week-long social isolation of mice after weaning was reported to induce impaired sociality (Makinodan et al., 2012) and reduced frequency of sEPSC and mEPSC in L5 pyramidal neurons of the mPFC that exhibited prominent hyperpolarization-activated cation currents (Yamamuro et al., 2018). Moreover, neonatal isolation in mice also decreased the amplitude of mEPSC in L2/3 pyramidal neurons of the mPFC and an increased percentage of wins in the social dominance tube test (Tada et al., 2016). Together with the results of the previous studies, our data strongly suggest that excitatory synaptic transmission in L2/3 pyramidal neurons of the mPFC contributes to social behavior in mice.

As for the behavioral phenotypes observed in *Setd1a* (+/−) mice but not in *Setd1a*-KD mice, it is possible that the contribution of brain regions other than the mPFC is required. Although the mPFC is thought to be involved in various behaviors such as sociality, working memory, and decision making (Euston et al., 2012; Grossmann, 2013), locomotor activity (Nagai et al., 2019; Bygrave et al., 2016), novel object recognition (Antunes and Biala, 2012), and avoidance behaviors (Padilla-Coreano et al., 2016) are likely to depend on other brain regions. Further studies are needed to determine the roles of *Setd1a* in brain regions other than the mPFC in mouse behavior. Another possible reason for the differences in behavioral phenotypes between *Setd1a* (+/−) and *Setd1a*-KD mice is the efficacy of *Setd1a* deletion from L2/3 pyramidal neurons of the mPFC in these 2 mouse

models. Considering that *Setd1a*-KD mice expressed *Setd1a*-KD vectors in only 30% of L2/3 pyramidal neurons of the mPFC (Figures S4E and S4F), it is possible that the proportion of *Setd1a*-KD neurons were too small to cause discernible deficits in mPFC-related behaviors other than sociality.

We conclude that excitatory synaptic function and structure in L2/3 pyramidal neurons of the mPFC are important for sociality and that *Setd1a* (+/−) mice would be a useful animal model for investigating the link among epigenomic factors, synaptic function, neural circuits, and SCZ-related behaviors. Moreover, the elucidation of signaling pathways for SETD1A-mediated regulation of synaptic function may provide potential novel targets for the treatment of SCZ patients.

STAR★METHODS

Detailed methods are provided in the online version of this paper and include the following:

- KEY RESOURCES TABLE
- RESOURCE AVAILABILITY
  - Lead Contact
  - Materials Availability
  - Data and Code Availability
- EXPERIMENTAL MODEL AND SUBJECT DETAILS
- METHOD DETAILS
  - Generation of Setd1a (+/–) mice
  - Vector construct
  - *In utero* electroporation
  - Electrophysiology
  - Validation of Setd1a-KD efficiency in HEK293T cells
  - ChIP sequencing
  - RNA sequencing
  - GO enrichment and protein-protein interaction network analyses
  - Quantification of GFP expression in bilateral Setd1a-Scr/KD mice
  - Quantitative reverse transcription-PCR
  - Western blotting
  - Immunostaining and dendritic spine morphology
  - Behavioral analyses
  - Open field test
  - Prepulse inhibition test and startle response
  - Sociality test
  - Reciprocal social interaction test
  - Y-maze spontaneous alteration test
  - Y-maze delayed alteration test
  - Object recognition test
  - Tail suspension test
  - Light/dark transfer test
  - Morris water maze test
  - Fear conditioning test
- QUANTIFICATION AND STATISTICAL ANALYSIS

SUPPLEMENTAL INFORMATION

Supplemental Information can be found online at https://doi.org/10.1016/j.celrep.2020.108126.

ACKNOWLEDGMENTS

We thank Y. Sugaya, Y. Hashimotodani, T. Akamatsu, H. Suzuki, T.-H. Kao, H. Sacai, and M. Choo for discussion and K. Matsuyama, M. Sekiguchi, M. Watanabe, and Y. Kato for technical assistance. We also thank H. Kimura (Tokyo Institute of Technology), N. Yakushiji-Kaminatsui, H. Sugishita, and H. Koseki (RIKEN) for analysis of the ChIP-seq data. This work was supported by Grants-in-Aid for Scientific Research (18H04012 and 19H05204 to M. Kano and 19H05253 to Y.K.) from the Japan Society for the Promotion of Science (JSPS) and by the Japan Agency for Medical Research and Development (AMED) under grant no. JP19dm0207071h.

AUTHOR CONTRIBUTIONS

K. Nagahama, T.W., N.U., and M. Kano designed the experiments and wrote the manuscript. K. Nagahama designed and performed the electrophysiology experiments, the construction of the plasmids, qPCR, the generation of the bilateral GFP expression mice, the immunohistochemical experiments, analysis of the RNA-seq data, and western blotting with the anti-H3K4me3 antibody. K.S. performed the behavioral experiments and analyses. K. Nagahama and K.K. performed western blotting with the anti-SETD1A antibody. M. Koebis, K. Nakao, and A.A. generated the *Setd1a* heterozygous mutant mice. Y.K. and Y.G. helped perform the western blotting with the anti-SETD1A antibody, analyzed the ChIP-seq data, and gave advice on RNA-seq.

DECLARATION OF INTERESTS

The authors declare no competing interests.

Received: January 22, 2020
Revised: June 17, 2020
Accepted: August 19, 2020
Published: September 15, 2020

REFERENCES

Ade, K.K., Janssen, M.J., Ortinski, P.I., and Vicini, S. (2008). Differential tonic GABA conductances in striatal medium spiny neurons. J. Neurosci. *28*, 1185–1197.

Ahmad, M., Polepalli, J.S., Goswami, D., Yang, X., Kaeser-Woo, Y.J., Südhof, T.C., and Malenka, R.C. (2012). Postsynaptic complexin controls AMPA receptor exocytosis during LTP. Neuron *73*, 260–267.

Akbarian, S., and Nestler, E.J. (2013). Epigenetic mechanisms in psychiatry. Neuropsychopharmacology *38*, 1–2.

Anastasiades, P.G., Marlin, J.J., and Carter, A.G. (2018). Cell-type specificity of callosally evoked excitation and feedforward inhibition in the prefrontal cortex. Cell Rep. *22*, 679–692.

Anders, S., and Huber, W. (2010). Differential expression analysis for sequence count data. Genome Biol. *11*, R106.

Antunes, M., and Biala, G. (2012). The novel object recognition memory: neurobiology, test procedure, and its modifications. Cogn. Process. *13*, 93–110.

Barch, D.M., and Ceaser, A. (2012). Cognition in schizophrenia: core psychological and neural mechanisms. Trends Cogn. Sci. *16*, 27–34.

Bellone, C., and Nicoll, R.A. (2007). Rapid bidirectional switching of synaptic NMDA receptors. Neuron *55*, 779–785.

Bledau, A.S., Schmidt, K., Neumann, K., Hill, U., Ciotta, G., Gupta, A., Torres, D.C., Fu, J., Kranz, A., Stewart, A.F., and Anastassiadis, K. (2014). The H3K4 methyltransferase Setd1a is first required at the epiblast stage, whereas Setd1b becomes essential after gastrulation. Development *141*, 1022–1035.

Boyden, E.S., Zhang, F., Bamberg, E., Nagel, G., and Deisseroth, K. (2005). Millisecond-timescale, genetically targeted optical control of neural activity. Nat. Neurosci. *8*, 1263–1268.

Boyle, A.P., Guinney, J., Crawford, G.E., and Furey, T.S. (2008). F-Seq: a feature density estimator for high-throughput sequence tags. Bioinformatics *24*, 2537–2538.

Bygrave, A.M., Masiulis, S., Nicholson, E., Berkemann, M., Barkus, C., Sprengel, R., Harrison, P.J., Kullmann, D.M., Bannerman, D.M., and Kätzel, D. (2016). Knockout of NMDA-receptors from parvalbumin interneurons sensitizes to schizophrenia-related deficits induced by MK-801. Transl. Psychiatry *6*, e778.

Choo, M., Miyazaki, T., Yamazaki, M., Kawamura, M., Nakazawa, T., Zhang, J., Tanimura, A., Uesaka, N., Watanabe, M., Sakimura, K., and Kano, M. (2017). Retrograde BDNF to TrkB signaling promotes synapse elimination in the developing cerebellum. Nat. Commun. *8*, 195.

Clapcote, S.J., Lipina, T.V., Millar, J.K., Mackie, S., Christie, S., Ogawa, F., Lerch, J.P., Trimble, K., Uchiyama, M., Sakuraba, Y., et al. (2007). Behavioral phenotypes of *Disc1* missense mutations in mice. Neuron *54*, 387–402.

dal Maschio, M., Ghezzi, D., Bony, G., Alabastri, A., Deidda, G., Brondi, M., Sato, S.S., Zaccaria, R.P., Di Fabrizio, E., Ratto, G.M., and Cancedda, L. (2012). High-performance and site-directed *in utero* electroporation by a triple-electrode probe. Nat. Commun. *3*, 960.

Diamantopoulou, A., and Gogos, J.A. (2019). Neurocognitive and perceptual processing in genetic mouse models of schizophrenia: emerging lessons. Neuroscientist *25*, 597–619.

Dillon, S.C., Zhang, X., Trievel, R.C., and Cheng, X. (2005). The SET-domain protein superfamily: protein lysine methyltransferases. Genome Biol. *6*, 227.

Ding, J.B., Oh, W.J., Sabatini, B.L., and Gu, C. (2011). Semaphorin 3E-Plexin-D1 signaling controls pathway-specific synapse formation in the striatum. Nat. Neurosci. *15*, 215–223.

Earls, L.R., Bayazitov, I.T., Fricke, R.G., Berry, R.B., Illingworth, E., Mittleman, G., and Zakharenko, S.S. (2010). Dysregulation of presynaptic calcium and synaptic plasticity in a mouse model of 22q11 deletion syndrome. J. Neurosci. *30*, 15843–15855.

Euston, D.R., Gruber, A.J., and McNaughton, B.L. (2012). The role of medial prefrontal cortex in memory and decision making. Neuron *76*, 1057–1070.

Fénelon, K., Xu, B., Lai, C.S., Mukai, J., Markx, S., Stark, K.L., Hsu, P.K., Gan, W.B., Fischbach, G.D., MacDermott, A.B., et al. (2013). The pattern of cortical dysfunction in a mouse model of a schizophrenia-related microdeletion. J. Neurosci. *33*, 14825–14839.

Franklin, K.B.J., and Paxinos, G. (2007). The mouse brain in stereotaxic coordinates, Third Edition (Academic Press).

Fromer, M., Pocklington, A.J., Kavanagh, D.H., Williams, H.J., Dwyer, S., Gormley, P., Georgieva, L., Rees, E., Palta, P., Ruderfer, D.M., et al. (2014). *De novo* mutations in schizophrenia implicate synaptic networks. Nature *506*, 179–184.

Fursova, N.A., Blackledge, N.P., Nakayama, M., Ito, S., Koseki, Y., Farcas, A.M., King, H.W., Koseki, H., and Klose, R.J. (2019). Synergy between variant PRC1 complexes defines polycomb-mediated gene repression. Mol. Cell *74*, 1020–1036.e8.

Gkogkas, C.G., Khoutorsky, A., Ran, I., Rampakakis, E., Nevarko, T., Weatherill, D.B., Vasuta, C., Yee, S., Truitt, M., Dallaire, P., et al. (2013). Autism-related deficits via dysregulated eIF4E-dependent translational control. Nature *493*, 371–377.

Glausier, J.R., and Lewis, D.A. (2013). Dendritic spine pathology in schizophrenia. Neuroscience *251*, 90–107.

Gonzalez-Burgos, G., Hashimoto, T., and Lewis, D.A. (2010). Alterations of cortical GABA neurons and network oscillations in schizophrenia. Curr. Psychiatry Rep. *12*, 335–344.

Greer, E.L., and Shi, Y. (2012). Histone methylation: a dynamic mark in health, disease and inheritance. Nat. Rev. Genet. *13*, 343–357.

Grossmann, T. (2013). The role of medial prefrontal cortex in early social cognition. Front. Hum. Neurosci. *7*, 340.

Grottick, A.J., Bagnol, D., Phillips, S., McDonald, J., Behan, D.P., Chalmers, D.T., and Hakak, Y. (2005). Neurotransmission- and cellular stress-related gene expression associated with prepulse inhibition in mice. Brain Res. Mol. Brain Res. *139*, 153–162.

Hardingham, N., and Fox, K. (2006). The role of nitric oxide and GluR1 in presynaptic and postsynaptic components of neocortical potentiation. J. Neurosci. *26*, 7395–7404.

Hashimoto, M., and Takemoto, T. (2015). Electroporation enables the efficient mRNA delivery into the mouse zygotes and facilitates CRISPR/Cas9-based genome editing. Sci. Rep. *5*, 11315.

Hayashi, M.K., Tang, C., Verpelli, C., Narayanan, R., Stearns, M.H., Xu, R.M., Li, H., Sala, C., and Hayashi, Y. (2009). The postsynaptic density proteins Homer and Shank form a polymeric network structure. Cell *137*, 159–171.

Hayashi-Takagi, A. (2017). Synapse pathology and translational applications for schizophrenia. Neurosci. Res. *114*, 3–8.

Hayashi-Takagi, A., Takaki, M., Graziane, N., Seshadri, S., Murdoch, H., Dunlop, A.J., Makino, Y., Seshadri, A.J., Ishizuka, K., Srivastava, D.P., et al. (2010). Disrupted-in-Schizophrenia 1 (DISC1) regulates spines of the glutamate synapse via Rac1. Nat. Neurosci. *13*, 327–332.

Huang, H.S., Matevossian, A., Whittle, C., Kim, S.Y., Schumacher, A., Baker, S.P., and Akbarian, S. (2007). Prefrontal dysfunction in schizophrenia involves mixed-lineage leukemia 1-regulated histone methylation at GABAergic gene promoters. J. Neurosci. *27*, 11254–11262.

Insel, T.R. (2010). Rethinking schizophrenia. Nature *468*, 187–193.

Jiang, W., Wei, M., Liu, M., Pan, Y., Cao, D., Yang, X., and Zhang, C. (2017). Identification of protein tyrosine phosphatase receptor type O (PTPRO) as a synaptic adhesion molecule that promotes synapse formation. J. Neurosci. *37*, 9828–9843.

Jones, C.A., Watson, D.J., and Fone, K.C. (2011). Animal models of schizophrenia. Br. J. Pharmacol. *164*, 1162–1194.

Jung, H., Park, H., Choi, Y., Kang, H., Lee, E., Kweon, H., Roh, J.D., Ellegood, J., Choi, W., Kang, J., et al. (2018). Sexually dimorphic behavior, neuronal activity, and gene expression in Chd8-mutant mice. Nat. Neurosci. *21*, 1218–1228.

Kanda, Y. (2013). Investigation of the freely available easy-to-use software 'EZR' for medical statistics. Bone Marrow Transplant. *48*, 452–458.

Kasai, H., Matsuzaki, M., Noguchi, J., Yasumatsu, N., and Nakahara, H. (2003). Structure-stability-function relationships of dendritic spines. Trends Neurosci. *26*, 360–368.

Klapoetke, N.C., Murata, Y., Kim, S.S., Pulver, S.R., Birdsey-Benson, A., Cho, Y.K., Morimoto, T.K., Chuong, A.S., Carpenter, E.J., Tian, Z., et al. (2014). Independent optical excitation of distinct neural populations. Nat. Methods *11*, 338–346.

Konopaske, G.T., Lange, N., Coyle, J.T., and Benes, F.M. (2014). Prefrontal cortical dendritic spine pathology in schizophrenia and bipolar disorder. JAMA Psychiatry *71*, 1323–1331.

Langmead, B., and Salzberg, S.L. (2012). Fast gapped-read alignment with Bowtie 2. Nat. Methods *9*, 357–359.

Langmead, B., Trapnell, C., Pop, M., and Salzberg, S.L. (2009). Ultrafast and memory-efficient alignment of short DNA sequences to the human genome. Genome Biol. *10*, R25.

Lazaro, M.T., Taxidis, J., Shuman, T., Bachmutsky, I., Ikrar, T., Santos, R., Marcello, G.M., Mylavarapu, A., Chandra, S., Foreman, A., et al. (2019). Reduced prefrontal synaptic connectivity and disturbed oscillatory population dynamics in the CNTNAP2 model of autism. Cell Rep. *27*, 2567–2578.e6.

Lewis, D.A., Hashimoto, T., and Volk, D.W. (2005). Cortical inhibitory neurons and schizophrenia. Nat. Rev. Neurosci. *6*, 312–324.

Love, M.I., Huber, W., and Anders, S. (2014). Moderated estimation of fold change and dispersion for RNA-seq data with DESeq2. Genome Biol. *15*, 550.

Maejima, T., Oka, S., Hashimotodani, Y., Ohno-Shosaku, T., Aiba, A., Wu, D., Waku, K., Sugiura, T., and Kano, M. (2005). Synaptically driven endocannabinoid release requires Ca^{2+}-assisted metabotropic glutamate receptor subtype 1 to phospholipase Cβ4 signaling cascade in the cerebellum. J. Neurosci. *25*, 6826–6835.

Makinodan, M., Rosen, K.M., Ito, S., and Corfas, G. (2012). A critical period for social experience-dependent oligodendrocyte maturation and myelination. Science *337*, 1357–1360.

Marissal, T., Salazar, R.F., Bertollini, C., Mutel, S., De Roo, M., Rodriguez, I., Müller, D., and Carleton, A. (2018). Restoring wild-type-like CA1 network dynamics and behavior during adulthood in a mouse model of schizophrenia. Nat. Neurosci. *21*, 1412–1420.

Matsuo, N., Takao, K., Nakanishi, K., Yamasaki, N., Tanda, K., and Miyakawa, T. (2010). Behavioral profiles of three C57BL/6 substrains. Front. Behav. Neurosci. *4*, 29.

Meechan, D.W., Tucker, E.S., Maynard, T.M., and LaMantia, A.S. (2009). Diminished dosage of 22q11 genes disrupts neurogenesis and cortical development in a mouse model of 22q11 deletion/DiGeorge syndrome. Proc. Natl. Acad. Sci. USA *106*, 16434–16445.

Mei, L., and Xiong, W.C. (2008). Neuregulin 1 in neural development, synaptic plasticity and schizophrenia. Nat. Rev. Neurosci. *9*, 437–452.

Mukai, J., Cannavò, E., Crabtree, G.W., Sun, Z., Diamantopoulou, A., Thakur, P., Chang, C.Y., Cai, Y., Lomvardas, S., Takata, A., et al. (2019). Recapitulation and reversal of schizophrenia-related phenotypes in *Setd1a*-deficient mice. Neuron *104*, 471–487.e12.

Nagai, J., Rajbhandari, A.K., Gangwani, M.R., Hachisuka, A., Coppola, G., Masmanidis, S.C., Fanselow, M.S., and Khakh, B.S. (2019). Hyperactivity with disrupted attention by activation of an astrocyte synaptogenic cue. Cell *177*, 1280–1292.e20.

Narushima, M., Hashimoto, K., and Kano, M. (2006). Endocannabinoid-mediated short-term suppression of excitatory synaptic transmission to medium spiny neurons in the striatum. Neurosci. Res. *54*, 159–164.

Niwa, M., Kamiya, A., Murai, R., Kubo, K., Gruber, A.J., Tomita, K., Lu, L., Tomisato, S., Jaaro-Peled, H., Seshadri, S., et al. (2010). Knockdown of DISC1 by in utero gene transfer disturbs postnatal dopaminergic maturation in the frontal cortex and leads to adult behavioral deficits. Neuron *65*, 480–489.

Ohno-Shosaku, T., and Kano, M. (2014). Endocannabinoid-mediated retrograde modulation of synaptic transmission. Curr. Opin. Neurobiol. *29*, 1–8.

Orlando, D.A., Chen, M.W., Brown, V.E., Solanki, S., Choi, Y.J., Olson, E.R., Fritz, C.C., Bradner, J.E., and Guenther, M.G. (2014). Quantitative ChIP-Seq normalization reveals global modulation of the epigenome. Cell Rep. *9*, 1163–1170.

Owen, M.J., Sawa, A., and Mortensen, P.B. (2016). Schizophrenia. Lancet *388*, 86–97.

Padilla-Coreano, N., Bolkan, S.S., Pierce, G.M., Blackman, D.R., Hardin, W.D., Garcia-Garcia, A.L., Spellman, T.J., and Gordon, J.A. (2016). Direct ventral hippocampal-prefrontal input is required for anxiety-related neural activity and behavior. Neuron *89*, 857–866.

Paoletti, P., Bellone, C., and Zhou, Q. (2013). NMDA receptor subunit diversity: impact on receptor properties, synaptic plasticity and disease. Nat. Rev. Neurosci. *14*, 383–400.

Peñagarikano, O., Abrahams, B.S., Herman, E.I., Winden, K.D., Gdalyahu, A., Dong, H., Sonnenblick, L.I., Gruver, R., Almajano, J., Bragin, A., et al. (2011). Absence of CNTNAP2 leads to epilepsy, neuronal migration abnormalities, and core autism-related deficits. Cell *147*, 235–246.

Polepalli, J.S., Wu, H., Goswami, D., Halpern, C.H., Südhof, T.C., and Malenka, R.C. (2017). Modulation of excitation on parvalbumin interneurons by neuroligin-3 regulates the hippocampal network. Nat. Neurosci. *20*, 219–229.

Pomarol-Clotet, E., Canales-Rodríguez, E.J., Salvador, R., Sarró, S., Gomar, J.J., Vila, F., Ortiz-Gil, J., Iturria-Medina, Y., Capdevila, A., and McKenna, P.J. (2010). Medial prefrontal cortex pathology in schizophrenia as revealed by convergent findings from multimodal imaging. Mol. Psychiatry *15*, 823–830.

Poo, M.M. (2001). Neurotrophins as synaptic modulators. Nat. Rev. Neurosci. *2*, 24–32.

Proepper, C., Johannsen, S., Liebau, S., Dahl, J., Vaida, B., Bockmann, J., Kreutz, M.R., Gundelfinger, E.D., and Boeckers, T.M. (2007). Abelson interacting protein 1 (Abi-1) is essential for dendrite morphogenesis and synapse formation. EMBO J. *26*, 1397–1409.

Ramos-Prats, A., Kölldorfer, J., Paolo, E., Zeidler, M., Schmid, G., and Ferraguti, F. (2019). An appraisal of the influence of the metabotropic glutamate 5 (mGlu5) receptor on sociability and anxiety. Front. Mol. Neurosci. *12*, 30.

Robinson, M.D., McCarthy, D.J., and Smyth, G.K. (2010). edgeR: a Bioconductor package for differential expression analysis of digital gene expression data. Bioinformatics *26*, 139–140.

Rodríguez-Tornos, F.M., Briz, C.G., Weiss, L.A., Sebastián-Serrano, A., Ares, S., Navarrete, M., Frangeul, L., Galazo, M., Jabaudon, D., Esteban, J.A., and Nieto, M. (2016). Cux1 enables interhemispheric connections of layer II/III neurons by regulating Kv1-dependent firing. Neuron *89*, 494–506.

Rothwell, P.E., Fuccillo, M.V., Maxeiner, S., Hayton, S.J., Gokce, O., Lim, B.K., Fowler, S.C., Malenka, R.C., and Südhof, T.C. (2014). Autism-associated neuroligin-3 mutations commonly impair striatal circuits to boost repetitive behaviors. Cell *158*, 198–212.

Sakai, H., Fujii, Y., Kuwayama, N., Kawaji, K., Gotoh, Y., and Kishi, Y. (2019). Plag1 regulates neuronal gene expression and neuronal differentiation of neocortical neural progenitor cells. Genes Cells *24*, 650–666.

Schizophrenia Working Group of the Psychiatric Genomics Consortium (2014). Biological insights from 108 schizophrenia-associated genetic loci. Nature *511*, 421–427.

Shen, L., Shao, N., Liu, X., and Nestler, E. (2014). ngs.plot: quick mining and visualization of next-generation sequencing data by integrating genomic databases. BMC Genomics *15*, 284.

Shorter, K.R., and Miller, B.H. (2015). Epigenetic mechanisms in schizophrenia. Prog. Biophys. Mol. Biol. *118*, 1–7.

Singh, T., Kurki, M.I., Curtis, D., Purcell, S.M., Crooks, L., McRae, J., Suvisaari, J., Chheda, H., Blackwood, D., Breen, G., et al.; Swedish Schizophrenia Study; INTERVAL Study; DDD Study; UK10 K Consortium (2016). Rare loss-of-function variants in *SETD1A* are associated with schizophrenia and developmental disorders. Nat. Neurosci. *19*, 571–577.

Skene, N.G., Bryois, J., Bakken, T.E., Breen, G., Crowley, J.J., Gaspar, H.A., Giusti-Rodriguez, P., Hodge, R.D., Miller, J.A., Muñoz-Manchado, A.B., et al.; Major Depressive Disorder Working Group of the Psychiatric Genomics Consortium (2018). Genetic identification of brain cell types underlying schizophrenia. Nat. Genet. *50*, 825–833.

Spruston, N. (2008). Pyramidal neurons: dendritic structure and synaptic integration. Nat. Rev. Neurosci. *9*, 206–221.

Sun, W., Poschmann, J., Cruz-Herrera Del Rosario, R., Parikshak, N.N., Hajan, H.S., Kumar, V., Ramasamy, R., Belgard, T.G., Elanggovan, B., Wong, C.C.Y., et al. (2016). Histone acetylome-wide association study of autism spectrum disorder. Cell *167*, 1385–1397.e11.

Szczurkowska, J., Cwetsch, A.W., dal Maschio, M., Ghezzi, D., Ratto, G.M., and Cancedda, L. (2016). Targeted *in vivo* genetic manipulation of the mouse or rat brain by *in utero* electroporation with a triple-electrode probe. Nat. Protoc. *11*, 399–412.

Tada, H., Miyazaki, T., Takemoto, K., Takase, K., Jitsuki, S., Nakajima, W., Koide, M., Yamamoto, N., Komiya, K., Suyama, K., et al. (2016). Neonatal isolation augments social dominance by altering actin dynamics in the medial prefrontal cortex. Proc. Natl. Acad. Sci. USA *113*, E7097–E7105.

Takata, A., Xu, B., Ionita-Laza, I., Roos, J.L., Gogos, J.A., and Karayiorgou, M. (2014). Loss-of-function variants in schizophrenia risk and *SETD1A* as a candidate susceptibility gene. Neuron *82*, 773–780.

Takata, A., Ionita-Laza, I., Gogos, J.A., Xu, B., and Karayiorgou, M. (2016). *De novo* synonymous mutations in regulatory elements contribute to the genetic etiology of autism and schizophrenia. Neuron *89*, 940–947.

Tanimura, A., Yamazaki, M., Hashimotodani, Y., Uchigashima, M., Kawata, S., Abe, M., Kita, Y., Hashimoto, K., Shimizu, T., Watanabe, M., et al. (2010). The endocannabinoid 2-arachidonoylglycerol produced by diacylglycerol lipase α mediates retrograde suppression of synaptic transmission. Neuron *65*, 320–327.

Uesaka, N., Mikuni, T., Hashimoto, K., Hirai, H., Sakimura, K., and Kano, M. (2012). Organotypic coculture preparation for the study of developmental synapse elimination in mammalian brain. J. Neurosci. *32*, 11657–11670.

Uesaka, N., Uchigashima, M., Mikuni, T., Nakazawa, T., Nakao, H., Hirai, H., Aiba, A., Watanabe, M., and Kano, M. (2014). Retrograde semaphorin signaling regulates synapse elimination in the developing mouse brain. Science *344*, 1020–1023.

Uesaka, N., Abe, M., Konno, K., Yamazaki, M., Sakoori, K., Watanabe, T., Kao, T.H., Mikuni, T., Watanabe, M., Sakimura, K., and Kano, M. (2018). Retrograde signaling from progranulin to Sort1 counteracts synapse elimination in the developing cerebellum. Neuron *97*, 796–805.e5.

Van Meer, P., and Raber, J. (2005). Mouse behavioural analysis in systems biology. Biochem. J. *389*, 593–610.

Xu, C., Krabbe, S., Gründemann, J., Botta, P., Fadok, J.P., Osakada, F., Saur, D., Grewe, B.F., Schnitzer, M.J., Callaway, E.M., and Lüthi, A. (2016). Distinct hippocampal pathways mediate dissociable roles of context in memory retrieval. Cell *167*, 961–972.e16.

Yamamuro, K., Yoshino, H., Ogawa, Y., Makinodan, M., Toritsuka, M., Yamashita, M., Corfas, G., and Kishimoto, T. (2018). Social isolation during the critical period reduces synaptic and intrinsic excitability of a subtype of pyramidal cell in mouse prefrontal cortex. Cereb. Cortex *28*, 998–1010.

Zhou, Y., Kaiser, T., Monteiro, P., Zhang, X., Van der Goes, M.S., Wang, D., Barak, B., Zeng, M., Li, C., Lu, C., et al. (2016). Mice with Shank3 mutations associated with ASD and schizophrenia display both shared and distinct defects. Neuron *89*, 147–162.

STAR★METHODS

KEY RESOURCES TABLE

REAGENT or RESOURCE	SOURCE	IDENTIFIER
Antibodies		
Mouse anti-H3K4me3	GeneTex, Inc.	CAT# GTX50897; RRID: in registration
Rabbit anti-H3K4me3	Sigma-Aldrich	CAT# 07-473; RRID: AB_1977252
Mouse anti-H3K4me3	MAB Institute, Inc.	CAT# MABI0304; RRID: 17012
Rabbit anti-histone H3	abcam	CAT# ab1791; RRID: AB_302613
Rabbit anti-hSETD1A	Bethyl	CAT# A300-289; RRID: AB_263413
Mouse anti-NeuN	Merck Millipore	CAT# MAB377; RRID: AB_2298772
Biological Samples		
HEK293T cell line	ATCC	CAT# CRL-3216; RRID: CVCL_0063
Chemicals, Peptides, and Recombinant Proteins		
NBQX	Tocris	CAT# 0373
D-AP5	Tocris	CAT# 0106
TTX	Nacalai Tesque	CAT# 32775-51
Picrotoxin	Nacalai Tesque	CAT# 28004-71
4-AP	Tocris	CAT# 02331-94
Deposited Data		
RNA-Seq (generated)	This paper	DDBJ: DRA010405
ChIP-Seq using anti-H3K4me3 antibody (generated)	This paper	DDBJ: DRA010404
ChIP-Seq using anti-H3K4me3 antibody (generated)	This paper	DDBJ: DRA010406
RNA-Seq (used in this study)	Mukai et al., 2019	GEO: GSE123652
ChIP-Seq using anti-SETD1A antibody (used in this study)	Mukai et al., 2019	GEO: GSE123652
Experimental Models: Organisms/Strains		
Mouse: *Setd1a* (+/−)	This study	N/A
Mouse: C57BL/6N	Japan SLC	N/A
Mouse: ICR	Japan SLC	N/A
Oligonucleotides		
Setd1a (+/−) gRNA 5′-GTGGATAGGAAGTATGGCGCTGG-3′	eurofins	N/A
Setd1a (+/−) genotyping F 5′-CTCGCCGCCATTTCTCTACATC-3′	eurofins	N/A
Setd1a (+/−) genotyping R 5′-CAGGTTCTGGAGGTTCTGGAG-3′	eurofins	N/A
Setd1a KD microRNA1 5′-TGCTGTTTGATATCAAGCTGGGCATGGTTTTGGCCACTGACTGACCATGCCCATTGATATCAAA-3′	eurofins	N/A
Setd1a KD microRNA1 5′-CCTGTTTGATATCAATGGGCATGGTCAGTCAGTGGCCAAAACCATGCCCAGCTTGATATCAAAC-3′	eurofins	N/A
Setd1a KD microRNA2 5′-TGCTGTTTGAAGGAGGTTGAAGTGGTGTTTTGGCCACTGACTGACACCACTTCCCTCCTTCAAA-3′	eurofins	N/A
Setd1a KD microRNA2 5′-CCTGTTTGAAGGAGGGAAGTGGTGTCAGTCAGTGGCCAAAACACCACTTCAACCTCCTTCAAAC-3′	eurofins	N/A
Setd1a Scr microRNA1 5′-TGCTGAGTTATGAACGTTGCGATTGCGTTTTGGCCACTGACTGACGCAATCGCAGTTCATAACT-3′	eurofins	N/A
Setd1a Scr microRNA1 5′-CCTGAGTTATGAACTGCGATTGCGTCAGTCAGTGGCCAAAACGCAATCGCAACGTTCATAACTC-3′	eurofins	N/A

(*Continued on next page*)

Continued

REAGENT or RESOURCE	SOURCE	IDENTIFIER
Setd1a Scr microRNA2 5′-TGCTGAGTGATAGGTAGGTTGATGTGGTTTTGGCCACTGACTGACCACATCAATACCTATCACT-3′	eurofins	N/A
Setd1a Scr microRNA2 5′-CCTGAGTGATAGGTATTGATGTGGTCAGTCAGTGGCCAAAACCACATCAACCTACCTATCACTC-3′	eurofins	N/A
Setd1a qRT-PCR F 5′-CCAACGAGAGTGTGCCCTTT-3′	eurofins	N/A
Setd1a qRT-PCR R 5′-CTGTCCATTGGCCTTTGGTG-3′	eurofins	N/A
GFP qRT-PCR F 5′-AAGCAGCACGACTTCTTCAAGTC-3′	eurofins	N/A
GFP qRT-PCR R 5′-TCGCCCTCGAACTTCACCTC-3′	eurofins	N/A
Ptpro qRT-PCR F 5′-CACTGCAGTGCGGGTGTG-3′	eurofins	N/A
Ptpro qRT-PCR R 5′-CTCGAATGTGTTGCAGGAGCCTG-3′	eurofins	N/A
Honer1 qRT-PCR F 5′-CACCAGCAAGCATGCAGTTACTG-3′	eurofins	N/A
Honer1 qRT-PCR R 5′-GTCATGTTTGGTGTGATGGTGC-3′	eurofins	N/A
Unc13c qRT-PCR F 5′-CTAAATTGTCAAATGCCCTGAAAAGCAC-3′	eurofins	N/A
Unc13c qRT-PCR R 5′-CTATGGAGAAGTTCCGGGTAGATG-3′	eurofins	N/A
Gapdh qRT-PCR F 5′-TGTGTCCGTCGTGGATCTGA-3′	eurofins	N/A
Gapdh qRT-PCR R 5′-TTGCTGTTGAAGTCGGAGGAG-3′	eurofins	N/A
Recombinant DNA		
pCAG-ChR2-P2A-mOrange	N/A	N/A
pCAG-FLEX-rc[Chronos-GFP]	Addgene	# 59056
pCAG-Cre-GFP	N/A	N/A
Software and Algorithms		
Bowtie2	Langmead and Salzberg, 2012	http://bowtie-bio.sourceforge.net/bowtie2/index.shtml
Bowtie	Langmead et al., 2009	https://sourceforge.net/projects/bowtie-bio/files/bowtie2/
F-seq	Boyle et al., 2008	http://fureylab.web.unc.edu/software/fseq/
ngs.plot	Shen et al., 2014	https://github.com/shenlab-sinai/ngsplot
DESeq v1.18.0	Anders and Huber, 2010	http://bioconductor.org/packages/release/bioc/html/DESeq.html
DESeq2 v1.6.3	Love et al., 2014	https://bioconductor.org/packages/release/bioc/html/DESeq2.html
EdgeR v3.4.6	Robinson et al., 2010	https://bioconductor.org/packages/release/bioc/html/edgeR.html
STRING	N/A	https://string-db.org/cgi/input.pl
ToppGene	N/A	https://toppgene.cchmc.org/
ImageJ	NIH	https://imagej.nih.gov/ij/
PATCHMASTER	HEKA	https://www.heka.com/
FITMASTER	HEKA	https://www.heka.com/
EZR	Kanda, 2013	http://www.jichi.ac.jp/saitama-sct/SaitamaHP.files/statmedEN.html
GraphPad Prism	GraphPad Software Inc	http://www.sigmaplot.co.uk/products/sigmaplot/sigmaplot-details.php
Venny 2.1	N/A	https://bioinfogp.cnb.csic.es/tools/venny/
BioRender	N/A	https://biorender.com/

RESOURCE AVAILABILITY

Lead Contact

Further information and requests for resources and reagents should be directed to and will be fulfilled by the Lead Contact, Masanobu Kano (mkano-tky@m.u-tokyo.ac.jp).

Materials Availability

Mouse line generated in this study and plasmids generated in this study for in utero electroporation are available upon reasonable requests.

Data and Code Availability

No code was generated in this study. Our RNA-seq (Figure 4) and ChIP-seq (Figure 4) data are available at DDBJ database (RNA-seq: DRA010405; ChIP-seq: DRA010404 and DRA010406). RNA-seq and ChIP-seq raw and processed data of Mukai et al. (2019) are available from GEO repository (GEO: GSE123652).

EXPERIMENTAL MODEL AND SUBJECT DETAILS

Setd1a (+/–) mice were generated in the C57BL6/N genetic background by clustered regularly interspaced short palindromic repeats and the associated proteins (CRISPR/Cas9) system. For *Setd1a*-KD experiments, we purchased pregnant ICR mice (E14) from SLC JAPAN. We used both male and female mice from P16 to P25 for electrophysiology, sex-matched pairs of mice at P30 for western blotting, qRT-PCR, RNA-Seq and ChIP-Seq, and 8-16 week-old male and female mice for behavioral analyses. All mice were group housed in a room under stable temperature and humidity on a 12 hour-light and dark cycle. Both water and food were supplied *ad libitum*. The animal experiments were approved by the Institutional Animal Care and Use Committee of The University of Tokyo and performed under the guidelines by the Japan Neuroscience Society.

METHOD DETAILS

Generation of Setd1a (+/–) mice

We selected a single guide RNA (sgRNA) targeting *Setd1a* gene using CRISPRdirect (http://crispr.dbcls.jp/). To prevent possible off-target effects of the system, we chose one target from five candidates with no homologous sequences on the other genes within 20 bases upstream of protospacer adjacent motif (PAM) and the cleaving efficiency of the sgRNA was validated with Guide-it™ sgRNA *In Vitro* Transcription and Screening Systems (Takara Bio USA, Inc., USA). The following target sequence at the exon 7 of *Setd1a* was selected, because frameshift mutation was identified in the exon 7 of *SETD1A* in a SCZ patient with several clinical symptoms (Singh et al., 2016; Takata et al., 2014): 5′-GTGGATAGGAAGTATGGCGCTGG-3′. Oocytes were collected from superovulated C57BL/6N female mice (CLEA Japan) and were *in vitro* fertilized with C57BL/6N sperms. Fertilized embryos were cryopreserved by vitrification at the pronuclear stage. After being thawed, morphologically normal embryos were collected in modified Whitten's medium (mWM) and perforated at the zona pellucida using an XYClone laser module (HAMILTON THORNE, MA, US). Cas9/gRNA ribonucleoprotein complex was delivered into embryos by electroporation as described previously with slight modifications (Hashimoto and Takemoto, 2015). The embryos were washed three times with Opti-MEM I (Thermo Fisher Scientific) supplemented with 0.1% polyvinyl alcohol (PVA) and once with 0.1% PVA-Opti MEM I containing Cas9 protein (20 ng/μl, Takara Bio) and sgRNA (15 ng/μl, Fasmac). Then the embryos were placed in a line in the gap of an electrode pair (LF501PT1-10, BEX, Tokyo, Japan) filled with the Cas9/gRNA-containing 0.1% PVA-Opti-MEM I (total 5 μL in volume) and electroporation was performed. Voltage pulses (30 V, 3 ms) were applied seven times at intervals of 100 ms using an electroporator CUY21EDIT II (BEX). After electroporation, the embryos were immediately collected from the electrode chamber and subjected to three washes with mWM. Electroporated embryos were transferred into oviducts of 0.5-day-post-coitum ICR recipients (Charles River Laboratories JAPAN). After birth, a direct sequencing was performed to identify the mutations of each pup. The pups had several types of mutations around the target sequence, and we selected a frameshift mutation (deletion of 1133-1134) in the exon 7 of *Setd1a* for further analyses. The mutant mice were identified by direct sequencing of the PCR products one by one.

Vector construct

We prepared all microRNA (miRNA) and cDNA expression vectors carrying fluorescent proteins (GFP or mOrange) using CAG promoter and all of them were validated by DNA sequencing. *Setd1a* cDNA sequence was obtained by reverse transcription-polymerase chain reaction (RT-PCR) from cDNA library made from the frontal cortex of mice at P30. The *Setd1a*-knockdown/scramble miRNA (KD/Scr miRNA) vectors were constructed with the BLOCK-iT Pol II miR RNAi expression vector kit (Invitrogen, CA, USA) with the following sequence according to the vector kit guidelines:

5′-TGCTGTTTGATATCAAGCTGGGCATGGTTTTGGCCACTGACTGACCATGCCCATTGATATCAAA-3′ and 5′-CCTGTTTGATATCAATGGGCATGGTCAGTCAGTGGCCAAAACCATGCCCAGCTTGATATCAAAC-3′ for *Setd1a*-KD miRNA-1;

5′-TGCTGTTTGAAGGAGGTTGAAGTGGTGTTTTGGCCACTGACTGACACCACTTCCCTCCTTCAAA-3′ and 5′-CCTGTTTGAAG GAGGGAAGTGGTGTCAGTCAGTGGCCAAAACACCACTTCAACCTCCTTCAAAC-3′ for *Setd1a*-KD miRNA-2;
5′-TGCTGAGTTATGAACGTTGCGATTGCGTTTTGGCCACTGACTGACGCAATCGCAGTTCATAACT-3′ and 5′-CCTGAGTTAT GAACTGCGATTGCGTCAGTCAGTGGCCAAAACGCAATCGCAACGTTCATAACTC-3′ for *Setd1a*-Scr miRNA-1;
5′-TGCTGAGTGATAGGTAGGTTGATGTGGTTTTGGCCACTGACTGACCACATCAATACCTATCACT-3′ and 5′-CCTGAGTGA TAGGTATTGATGTGGTCAGTCAGTGGCCAAAACCACATCAACCTACCTATCACTC-3′ for *Setd1a*-Scr miRNA-2

Setd1a cDNA rescue vector (*Setd1a*-Res vector) was made with QuikChange lightning site-directed mutagenesis kit (Agilent Technologies, CA, USA). We inserted mutation into the KD miRNA target sequences without codon alteration and inhibited binding of the KD miRNA to the rescue vector. *Setd1a*-Res vector was tagged to mOrange and picornavirus "self-cleaving" P2A peptide sequence was inserted between *Setd1a* cDNA and mOrange sequence to get strong bicistronic expression.

For optogenetic experiments with channelrhodopsin-2 (ChR2), we constructed the pCAG-ChR2-P2A-mOrange vector using ChR2 sequence cloned from pLenti-CaMK2α-ChR2-eYFP (Boyden et al., 2005). pCAG-FLEX-rc[Chronos-GFP] was a gift from Edward Boyden (Addgene plasmid # 59056) (Klapoetke et al., 2014). Because the Chronos plasmid expressed GFP signal in a Cre-dependent manner, pCAG-KD-miRNA-mOrange vectors against *Setd1a* were constructed with the KD-miRNA sequences subcloned from the KD plasmids with GFP as shown above.

In utero electroporation

We used ICR mice at E14.5 for in utero electroporation (SLC JAPAN) to target L2/3 pyramidal neurons (Niwa et al., 2010). The pregnant mice were deeply anesthetized with sodium pentobarbital (Somnopentol; Kyoritsu Seiyaku Co., Tokyo, Japan or Nacalai tesque) during the surgery. The plasmids were injected into a lateral ventricle and delivered by electrical stimulation (35 V for 50 ms, 5 times at 950 ms intervals) via forceps-shaped electrodes (CUY650P5, Unique Medical Imada, Aichi, Japan) connected to an electroporator (CUY21, NepaGene, Chiba, Japan) for electrophysiological and morphological analyses of *Setd1a*-KD neurons. For behavioral analyses, bilateral *Setd1a*-KD mice were generated by in utero electroporation with a triple-electrode probe reported previously (dal Maschio et al., 2012; Szczurkowska et al., 2016). According to these reports, we prepared the "triceps-electrodes" that were made of the forceps-shaped electrodes as shown in Figure S6. The concentration of injected DNA plasmid was adjusted to 2.0-3.0 μg/μl with a phosphate-buffered saline (PBS) solution. After birth, the fluorescent expression in each pup was verified through the skull with green or red light glasses, and pups were selected when they had an efficient fluorescent expression.

Electrophysiology

Prefrontal coronal slices of 300 μm thickness were cut from P16-P25 mice in the following cutting solution; 120 mM Choline Cl, 28 mM $NaHCO_3$, 1.25 mM NaH_2PO_4, 2 mM KCl, 25 mM glucose, 1 mM $CaCl_2$, 8 mM $MgCl_2$, bubbled with 95% O_2 and 5% CO_2 with a vibratome slicer (Leica, Germany) (Narushima et al., 2006). The slices were incubated at room temperature for 30-60 min with artificial cerebrospinal fluid (ACSF) containing 125 mM NaCl, 2.5 mM KCl, 2 mM $CaCl_2$, 1 mM $MgSO_4$, 1.25 mM NaH_2PO_4, 26 mM $NaHCO_3$, and 20 mM glucose bubbled with 95% O_2 and 5% CO_2 (Choo et al., 2017; Uesaka et al., 2012, 2014, 2018).

For whole-cell patch clamp recording, we identified layer 2/3 pyramidal neurons of the mPFC morphologically or by fluorescence with Olympus BX51WI microscope (Olympus). We recorded from GFP-positive neurons with *Setd1a* KD and GFP-negative control neurons in the same slices. The pipet resistance was 2.4-5 MΩ when filled with an internal solution containing 120 mM $CsMeSO_3$, 15 mM CsCl, 8 mM NaCl, 0.2 mM EGTA, 10 mM HEPES, 10 mM TEA-Cl, 4 mM MgATP, 0.3 mM Na_2GTP, 0.1 mM Sperimine, 5 mM QX314 (pH 7.3, adjusted with CsOH) (Ding et al., 2011) for recording amplitude of evoked postsynaptic currents to estimate the input-output relation, paired pulse ratio (PPR), and inhibition/excitation (I/E) balance. For voltage-clamp recording of spontaneous and miniature excitatory postsynaptic currents (sEPSCs and mEPSCs) and for current-clamp recordings to analyze firing properties, we used an internal solution composed of 130 mM K D-gluconate, 6 mM KCl, 10 mM NaCl, 10 mM HEPES, 0.16 mM $CaCl_2$, 2 mM $MgCl_2$, 0.5 mM EGTA, 4 mM Na-ATP, and 0.4 mM Na-GTP (pH 7.3, adjusted with KOH) (Maejima et al., 2005). For recording spontaneous and miniature inhibitory postsynaptic currents (sIPSCs and mIPSCs), an internal solution with the following composition was used: 145 mM KCl, 10 mM HEPES, 10 mM EGTA, 0.16 mM $CaCl_2$, 2 mM $MgCl_2$, 5 mM Mg-ATP, and 0.2 mM Na-GTP (pH 7.2, adjusted with KOH) (Ade et al., 2008). All of the recordings were performed at 30-32°C with an EPC-10 amplifier (HEKA Elektronik, Lambrecht/Pfalz, Germany). Data was filtered at 2.9 kHz and digitized at 20 kHz. During recording, the access resistance was compensated by 70%. 5-10 traces were averaged in each recording for assessing input-output relation and PPR, and 20-30 traces were averaged for I/E balance. Parameters from current-clamp recordings were calculated by averaging the values from 3 consecutive action potential traces for each injected current.

EPSCs were evoked by local electrical stimulation through a bipolar tungsten stimulating electrode (PHC, Inc, USA). Evoked AMPAR-mediated EPSCs were recorded at holding potential of −70 mV in the presence of 0.1 mM picrotoxin (PTX) (Nacalai Tesque, Kyoto, Japan), whereas evoked-NMDAR-mediated EPSCs were recorded at +40 mV in the presence of 0.1 mM picrotoxin and 10 μM 2,3-dihydroxy-6-nitro-7-sulfamoyl-benzo [f] quinoxaline (NBQX) (Nacalai Tesque). The stimulating electrode was placed 50-100 μm away from the recorded neurons. Paired electrical stimuli for PPR were delivered with inter-stimulus interval of 20, 50, 100, and 500 ms. Inhibitory/excitatory ratio was measured as reported previously (Rothwell et al., 2014). In brief, evoked EPSCs were recorded at −40 mV, the Cl^- equilibrium potential in our experimental condition, in the presence of 50 μM D-AP5 (Nacalai

Tesque). Then, evoked EPSCs were suppressed by adding 10 μM NBQX to the bath and the holding potential was set at 0 mV, the reversal potential of EPSC. Under this condition, evoked IPSCs were recorded, which was confirmed by PTX (0.1 mM)-blockade of the responses. The liquid junction potential was corrected when assessing I/E balance and measuring resting membrane potential. mEPSCs and mIPSCs were recorded at −70 mV in the presence of 0.5 μM tetrodotoxin (TTX) (Nacalai Tesque) with 0.1 mM PTX (for mEPSC) or with 10 μM NBQX plus 50 μM D-AP5 (for mIPSC). sEPSCs and sIPSCs were recorded in the presence of 0.1 mM PTX (for sEPSC) or 10 μM NBQX plus 50 μM D-AP5 (for sIPSC). For analyzing data of spontaneous and miniature synaptic currents, we used Mini Analysis program (Synaptosoft). Individual synaptic events were detected by eye when the amplitude was larger than 5 pA and the rise time was faster than 3 ms. The decay of NMDA receptor (NMDAR)-mediated excitatory synaptic current was fitted to a double exponential equation and weighted tau (τ_W) was calculated by the following formula: $\tau_W = [(I_s \times \tau_s) + (I_f \times \tau_f)]/(I_s + I_f)$, where I_s and I_f were the amplitudes and τ_s and τ_f were decay time constants of slow and fast components of NMDAR-mediated currents, respectively (Polepalli et al., 2017; Ahmad et al., 2012).

The PATCHMASTER and FITMASTER programs (HEKA, Germany) were used for the analyses of other parameters.

In experiments with optogenetic stimulation, ChR2 was transfected into L2/3 pyramidal neurons in the mPFC by in utero electroporation with the *Setd1a*-Scr or *Setd1a*-KD microRNA vector (Figure 6D). To sparsely express Chronos in a subset of *Setd1a*-KD neurons, 1-2 μg/μl of pCAG-DIO-Chronos-GFP plasmid and the same dose (1-2 μg/μl) of pCAG-KD-mOrange plasmid were transfected with a smaller dose (0.5-0.75 ng/μl) of pCAG-Cre-GFP plasmid into L2/3 pyramidal neurons. This procedure resulted in expression of Cre recombinase in a subset of L2/3 pyramidal neurons that express floxed Chronos and GFP together with microRNA against *Setd1a* and mOrange. Thus, Chronos and GFP were expressed sparsely among mOrange-positive L2/3 pyramidal neurons with *Setd1a* KD (Figures 6D and S4G). A 465 nm blue LED light pulse (4 mW/mm^2, 2 or 10 ms) (Anastasiades et al., 2018; Xu et al., 2016) was used as optical stimulation from LEX2-LZ4-B (Brainvision, Inc., Tokyo, Japan). Paired light pulse stimuli were applied at 50, 100, 500 ms of inter-flash intervals (IFI) for ChR2, and at 20, 25, 50, 100, 500 ms of IFI for Chronos.

Validation of Setd1a-KD efficiency in HEK293T cells

We used HEK293T cells to validate *Setd1a*-KD efficiency (Choo et al., 2017; Uesaka et al., 2012, 2014, 2018). The microRNA vectors were transfected into the cells with wild-type or rescue vector of *Setd1a* cDNA by X-tremeGENE 9 reagents (Roche, Basel, Switzerland). An efficiency of KD miRNA vectors was validated with quantification of mOrange intensity normalized to GFP. We also checked the signal of *Setd1a*-rescue vector with the KD miRNA to assess the resistance of the rescue vector. The fluorescent signals were validated with a confocal microscope (FV1200, Olympus) and the images were analyzed with ImageJ (NIH, USA).

ChIP sequencing

The prefrontal cortices from *Setd1a* (+/+) and *Setd1a* (+/–) mice were cut into small pieces (~1 mm) and fixed with 4% paraformaldehyde (PFA)/PBS at room temperature for 10 min. Chromatin immunoprecipitation (ChIP) for H3K4me3 was performed as previously described (Sakai et al., 2019), using an antibody against H3K4me3 (MBL, MABI0304) with mixing HEK293T cells as spike-in genome. Template preparation for IP samples was conducted using QIAseq Ultralow Input Library Kit (QIAGEN) according to the manufacturers' instructions and constructed template was used for the deep sequencing analysis on the Illumina HiSeq platform by 150-base-paired-end read. Template preparation for IP samples for determining the ratio of mouse and human cell numbers was conducted using TDE1 enzyme (Illumina) and constructed template was used for the deep sequencing analysis on the Illumina Novaseq6000 platform by 150-base-paired-end read. The sequence data were deposited in the DNA Data Bank of Japan (DDBJ) Sequence Read Archive. Down-sampled 18 million sequences were used for the following analysis. Sequences were mapped to the reference mouse-human hybrid genome (mm10-hg38) using bowtie2 software (Langmead and Salzberg, 2012). For determining SETD1A-bound regions, public sequence data (SRR10254727 and SRR10254728) were mapped to reference mouse genome (mm10) using bowtie software (Langmead et al., 2009). We only used uniquely mapped and deduplicated reads with no base mismatch. SETD1A peaks were called using F-seq software (Boyle et al., 2008). Read count per million mapped reads (RPM) around SETD1A peaks or SETD1A-bound TSS were analyzed by ngs.plot software (Shen et al., 2014). The ratio of IP and input read numbers between mouse and human cells were used for global normalization as previously reported (Fursova et al., 2019; Orlando et al., 2014).

RNA sequencing

Total RNA was extracted from the frontal cortical tissues of 1-month-old mice using RNeasy mini kit (QIAGEN) and Sepasol®-RNA I Super G (Nacalai Tesque). The RNA sequencing of messenger RNA (mRNA) and analyses of the gene expression were performed by GENEWIZR. The RNA of each sample was quantified and qualified by Agilent 2100 Bioanalyzer (Agilent Technologies, Palo Alto, CA, USA), NanoDrop (Thermo Fisher Scientific Inc.) and 1% agarose gel. 1 μg of total RNA with RIN value above 7 was used for the following library preparation, which is performed with NEBNext® Ultra Directional RNA Library Prep Kit for Illumina. Complementary DNA was sequenced with an Illumina HiSeq instrument (Illumina). The sequenced data was analyzed by the fragments per kilobase of exon per million reads mapping (FPKM). Differential expression analysis was performed with the DESeq Bioconductor package. Threshold of p value in each gene was under 0.05 to detect differentially expressed (DE) genes between *Setd1a* (+/+) and *Setd1a* (+/–) mice. Using the previous RNA-Seq data of Mukai et al. (GEO: GSE123652), we examined the overlapped genes between both RNA-Seq data by Venny 2.1 online program (https://bioinfogp.cnb.csic.es/tools/venny/).

GO enrichment and protein-protein interaction network analyses

We performed gene ontological enrichment analysis of up and downregulated DE genes in *Setd1a* (+/−) mice to analyze the overlap between DE genes and the Gene ontology (GO) annotations in the STRING (https://string-db.org/cgi/input.pl) for the annotations related to biological functions and the ToppGene online program (https://toppgene.cchmc.org/) for those related to neurodevelopmental disorders. Protein-protein interaction network analysis was performed in the STRING program. *P*-values in each enrichment analysis were adjusted by Benjamini and Hochberg's approach.

Quantification of GFP expression in bilateral Setd1a-Scr/KD mice

For quantification of GFP-positive area in mice with bilateral GFP expression, randomly selected mice were sacrificed after the behavioral tests (10-18 weeks) under 10% pentobarbital anesthesia followed by perfusion fixation with paraformaldehyde in 0.1 M phosphate buffer. Image analysis was performed with ImageJ (NIH). Coronal PFC slices (100 μm) were cut at +2.34, +1.94, +1.18, +0.98, and –1.34 mm from Bregma (Niwa et al., 2010). Images were captured with a confocal microscope (FV1200, Olympus) and proportions of areas with GFP signal were quantified in the following brain regions; mPFC, dorsolateral prefrontal cortex (DLPFC), orbitofrontal cortex (OFC), motor cortex (mCx), sensory cortex (sCx), cingulate cortex (cgCx), retrosplenial cortex (rsCx), and other areas. These areas were identified by landmarks and neuroanatomical nomenclature with the atlas of Franklin and Paxinos (2007). The proportion of GFP area was calculated by dividing the area with GFP signal by the total area for each cortical region.

To measure the proportion of GFP-positive neurons in layer 2/3, we performed immunostaining with rat anti-GFP antibody (1:1000, Nacalai Tesque, Kyoto, Japan) and mouse anti-CaMKII antibody (1:300, Abcam, Cambridge, UK). After the mice were sacrificed at P24, we cut mPFC coronal slices with 50 μm thickness and performed permeabilization with 0.5% triton-X followed by blockade with 10% donkey serum. Thereafter, we applied antibodies against GFP and CaMKII at 4°C overnight and then secondary antibody (anti-rat IgG Alexa Fluor 488 antibody; 1:300 and anti-mouse Alexa Fluor antibody; 1:300, Life Technologies, Inc.) at room temperature for 2-3 hours. To prevent bleaching of fluorescent signals and staining nucleic acid, we used VECTASHIELD Hard set with DAPI (Vector Laboratories, Inc. Burlingame, USA).

Quantitative reverse transcription-PCR

We performed real-time PCR with reverse transcription to quantify expression level of mRNA for *Setd1a* and GFP. Prefrontal coronal slices were cut similarly to slices for electrophysiological experiments. The GFP-positive areas of the mPFC were excised from the slices and frozen with liquid nitrogen. Total RNA was purified and reverse transcription was conducted with the PrimeScript 1st Strand cDNA Synthesis Kit (TaKaRa). Real-time PCR was performed with LightCycler 480 SYBR Green I Master (Roche Molecular Systems, Inc. Basel, Switzerland) in LightCycler 480 System II (Roche Molecular Systems). The primers for qPCR were as follows: 5′-CCAACGAGAGTGTGCCCTTT-3′ (forward), 5′-CTGTCCATTGGCCTTTGGTG-3′ (reverse) for *Setd1a*, 5′-CACTGCAGTGCGGGTGTG-3′ (forward), 5′-CTCGAATGTGTTGCAGGAGCCTG-3′ (reverse) for *Ptpro*, 5′-CACCAGCAAGCATGCAGTTACTG-3′ (forward), 5′-GTCATGTTTGGTGTGATGGTGC-3′ (reverse) for *Homer1*, 5′-CTAAATTGTCAAATGCCCTGAAAAGCAC-3′ (forward), 5′-CTATGGAGAAGTTCCGGGTAGATG-3′ (reverse) for *Unc13c* and 5′-AAGCAGCACGACTTCTTCAAGTC-3′ (forward), 5′-TCGCCCTCGAACTTCACCTC-3′ (reverse) for GFP. For normalization of the mRNA level, a housekeeping gene, *Gapdh,* was used as a standard with the following sequences: 5′-TGTGTCCGTCGTGGATCTGA-3′ (forward), 5′-TTGCTGTTGAAGTCGGAGGAG-3′ (reverse) (Uesaka et al., 2018). $2^{-\Delta\Delta Ct}$ method was applied for the quantification of mRNA (Applied Biosystems).

Western blotting

Protein samples for the western blotting were extracted from the prefrontal cortex tissues of 1-month mice. The samples were homogenized in RIPA buffer (Nacalai Tesque) or a hand-made solution composed of 50 mM Tris-HCl (pH 7.5), 150 mM NaCl, 1mM EDTA, 1% NP-40, 0.1% sodium deoxycholate, 0.1% SDS, 1 mM dithiothreitol, and 5% aprotinin. The 5-10 μg protein was applied to the gel electrophoresis with the membrane, which was then blocked in BLOCKING ONE (Nacalai Tesque). The membrane was stained with the primary antibodies against SETD1A (Rabbit, 1:500-1000, A300-289A, Bethyl), tri-methylated lysine 4 of histone H3 (Rabbit, 1:1000, Sigma-Aldrich), and histone H3 (Rabbit, 1:5000, abcam) in 4°C overnight. After three-times wash with phosphate-buffered saline (PBS) with Tween 20, the membrane was incubated with the horseradish peroxidase–conjugated secondary antibody (Rabbit, 1:20000, abcam). The chemiluminescence was induced by Chemi-Lumi One L (Nacalai Tesque), which was then captured by an ImageQuant LAS 4000 instrument (GE Healthcare). The quantification of the band signals was performed with ImageQuant TL (GE Healthcare) and the signal of SETD1A was normalized to that of histone H3.

Immunostaining and dendritic spine morphology

To quantify the density and morphological parameters of spine in *Setd1a* (+/–) mice, we injected a neurobiotin into each neuron in acute coronal mPFC slices (300 μm) through a patch pipette to observe individual spines, which was perfused in the 4% paraformaldehyde at 4°C overnight. Then, the slices were incubated with the streptavidin with DyLight 594 (1:300, Funakoshi Co., Ltd., Japan) at 4°C for 2-3 days.

To assess the spine morphology of the *Setd1a*-Scr or *Setd1a*-KD neurons expressing GFP, mOrange was expressed sparsely in a subset of the *Setd1a*-Scr or *Setd1a*-KD neurons by Cre-dependent recombination (Rodríguez-Tornos et al., 2016). In utero

electroporation was performed with pCAG-DIO-mOrange (1.0-1.5 μg/μl), pCAG-Cre-GFP (0.5-0.75 ng/μl) and *Setd1a*-Scr or *Setd1a*-KD vector (2.0 μg/μl) at E14.5. For immunohistochemistry, the mice were sacrificed at P24 in the same way as shown above and mPFC coronal slices were cut with 50-100 μm in thickness. The slices were incubated with a rat anti-GFP antibody (1:1000; Nacalai Tesque) and a rabbit anti-RFP antibody (1:300; MBL Aichi, Japan) at 4°C overnight. After washing, an anti-rat IgG Alexa Fluor 488 antibody and an anti-rabbit IgG Alexa Fluor 647 antibody (1:300; Life Technologies) were used for GFP and mOrange staining, respectively, for 2-3 hours at room temperature.

We captured mPFC images using confocal microscopy (FV1200, Olympus) with 60 × oil immersion objective using digital zoom 2.0 at 0.48 μm-z series (1024 × 1024 pixels resolution). To detect spines from the images, we used Neurolucida360 software (MBF Bioscience, Williston, Vt., USA) and defined them automatically with the same criteria (outer range: 2.5 μm, minimum height: 0.3 μm, detector sensitivity: 50%, minimum count: 10 voxels for detecting spines and head-to-neck ratio: 1.1, length-to-head ratio: 2.5, mushroom head size: 0.35 μm, filopodium length: 3 μm for the classification of spines).

To observe the layer structure of the mPFC, NeuN signal was visualized by immunostaining with a mouse anti-NeuN antibody (1:300, Merck Millipore, Germany). The images of the mPFC were captured as shown above. The frequency distribution of NeuN labeled cells was assessed across 12 equal bins (60 μm / bin) from the pia to deep layers of the PFC. Quantification of the number of NeuN positive neurons was performed with ImageJ (NIH, USA) (Meechan et al., 2009).

Behavioral analyses

All of the behavioral tests were performed using age-matched adult mice (8-16 weeks) for wild-type and *Setd1a* (+/–) mice or for bilateral *Setd1a*-Scr and-KD mice on light-on periods. Before the experiments, the mice were habituated in the testing areas for at least 60 min.

Open field test

Horizontal activity in a small open field apparatus (30 × 30 × 40 cm, W x D x H) was measured for 30 min. The trial was repeated for three consecutive days. We measured the total distance traveled in each trial day and compared the values between different genotypes. Behavior was video-recorded from above, and horizontal activity was analyzed with TimeOF4 software (O'Hara & Co, Japan).

Prepulse inhibition test and startle response

To test startle response and prepulse inhibition, a mouse was put into a plastic tube (35 mm diameter, 12 cm long) which was placed on a sensor block in a soundproof chamber. 65 dB white noise was presented as background noise in the chamber. In the first session, to test auditory startle response, mice were exposed to white noise at various tone intensity. In this session, 70, 75, 80, 85, 90, 95, 100, 110 or 120 dB white noise (40 ms) was presented in random order and with random interval (10 to 20 s) for five times. In the second session, to test prepulse inhibition, mice were exposed to 120 dB tone with various intensity of pre-tone. In this session, mice were exposed to five different trials: no stimulus, 120 dB startle stimulus only, 70 dB prepulse and 120 dB startle stimulus, 75dB prepulse and 120 dB startle stimulus, and 80 dB prepulse and 120 dB startle stimulus. The trials were repeated for 10 times in random orders and with random intervals (10 to 20 s). The startle data were analyzed with AnimalStartle software (O'Hara & Co, Japan). The inhibition of startle response was calculated with the following equation: 100 – [(startle response to each prepulse)/(startle response to 120 dB pulse)] × 100.

Sociality test

The sociality test was performed in the open field apparatus (50 × 50 × 40 cm, W x D x H) with 15 lx luminance. The test consisted of a 10-min habituation session, a 3-min interval, and a 10-min test session. In the habituation session, mice were allowed to explore the open field freely. In the test session, two empty cylinder wire cages (10 cm in diameter, 15 cm high) were placed in two adjacent corners. One wire cage contained a novel mouse (7-week-old male DBA2, purchased from Nihon SLC) and the other was empty (empty cage), and a test mouse was set in the open field arena. To assess staying time around the novel mouse in the cage, mouse behavior was video-recorded from above and the times spent in the two corner areas containing the cylinders (16.7 × 16.7 cm square) were analyzed automatically with TimeOF4 software (O'Hara & Co, Japan). Social preference was assessed by the following equation: Preference index = $(T_{mouse} - T_{cage})/(T_{mouse} + T_{cage})$ where T_{mouse} and T_{cage} are the staying time around the mouse cage and that around the empty cage, respectively (Ramos-Prats et al., 2019). We compared T_{mouse}, T_{cage} and preference index between *Setd1a* (+/+) and *Setd1*a (+/+) mice, and between *Setd1a*-Scr and *Setd1*a-KD mice. After each test session, the cylinder wire cages were extensively washed with water.

Reciprocal social interaction test

The reciprocal social interaction was analyzed as shown in the previous report (Gkogkas et al., 2013). A test mouse was placed at one of the corners in an open field (50 × 40 × 50 cm, 15 lux), while an adult male DBA2 mouse (SLC JAPAN) was on the other side. We monitored how the test mouse contacted with the novel DBA2 mouse using a video camera located above the open field during 5-min trial. The number of active and passive contacts were measured in each test mouse.

Y-maze spontaneous alteration test

The maze consisted of three arms, each being 40 cm long, 12 cm high, and 3 cm wide at the bottom, and with the same length and height but 10 cm wide at the top. The arms converged at an equilateral triangular central area whose longest axis was 4 cm. Each mouse was placed at the center of apparatus and allowed to move freely through the maze for 7 min. Mouse behavior was recorded with video camera from above and arm entry was analyzed with TimeYM1 software (O'Hara & Co, Japan). We assessed how many times a mouse entered different arms consecutively (alteration). Alternation was defined as a consecutive entry into each of the three different arms. The alternation rate (%) was calculated as follows: [the number of consecutive entries into three different arms/(the number of total arms entered – 2)] × 100 (%).

Y-maze delayed alteration test

The Y-maze delayed alteration test was performed in a modified Y-maze. Feeding arenas (10 × 10 cm) were attached to the ends of two arms of the Y-maze. Another arm was used as the start arm. Body weights of mice were controlled to 80%–85% from baseline weights by restricting the food access throughout the experiments. Before training session, mice were habituated to the Y-maze in which a food pellet (20 mg) was placed in each feeding arena for 4 days. The test was composed of a training (forced alteration) session followed by a delayed alteration session. In the training (forced alteration) session, as a sample run, mice set on a start arm of the maze were forced to choose one arm in which food pellet was placed in the feeding arena. After eating, as a choice run, mice were returned to the start arm and allowed to take a free choice of the two arms. If mice chose the opposite arm, they were able to eat the food pellet placed in the feeding arena. If mice chose the same arm, they were returned to the start arm without food reward. Mice were trained in 6 trials per day for 5 days. 5-10 s interval was inserted between the sample run and the choice run. During the delayed alteration session, 10, 30, and 60 s intervals were inserted between the sample run and the choice run in each trial. The trials with each of the three intervals were exerted twice a day, which was repeated for 4 days. The percentage of correct choice at choice run was calculated in each trial of the training and the delayed alteration sessions.

Object recognition test

This test was performed in an open field test apparatus (50 × 50 × 40 cm, W x D x H) with 15 lx luminance. The test was composed of a 10-min training (learning) session, 1- and 24-hour intervals, and 10-min test sessions. In the training session, a mouse was allowed to explore the open field freely in which the same objects were located in two adjacent corners (i.e., object A versus object A). In the test session, 1 or 24 hours after the training session, the mouse was allowed to explore the arena again in which one of the objects was replaced with a different one (i.e., object A versus object B). Mouse behavior was video-recorded from above, and the times spent in the area (16.7 × 16.7 cm square) around each of the two objects were measured with TimeOF4 software (O'Hara & Co, Japan).

Tail suspension test

Individual mice were suspended by their tails using self-adhesive tape from a small hook at one end of wire for 10 min. Mouse behavior was recorded with a video camera. The duration of immobility, which was analyzed automatically and calculated in 1 min bins, and the latency to immobility was measured with TimeFZ2 software (O'Hara & Co, Japan). Grayscale video images were converted into black and white binary images and a mouse was detected as a black object that consisted of about 4000 to 5500 pixels. By comparing two consecutive binary images of a mouse taken at 0.5 s interval, change in the posture of the mouse was detected as a change in the shape of the object. If the mismatch of the object shape was less than 400 pixels, the mouse was judged to show "immobility." The percentage of immobility in each 1 min bin was calculated by dividing the immobility time by 1 min.

Light/dark transfer test

The apparatus was consisted of a light box (made of white plastic, 20 × 20 × 20 cm, illuminated by 250 lx LEDs) and a dark box (made of black plastic, 20 × 20 × 20 cm, not illuminated) with a CCD camera attached to the ceiling of each box. In this test, mice were introduced into the dark box and allowed to move freely between the boxes for 10 min. Mice were allowed to choose the boxes through a tunnel located on the center panel between the two boxes (3 × 5 cm). Percentage of time spent in the light box, and the latency to first move into the light box were measured and compared between *Setd1a* (+/+) and *Setd1*a (+/+) mice, and between *Setd1a*-Scr and *Setd1*a-KD mice. The data were collected and analyzed with TimeLD4 software (O'Hara & Co, Japan)

Morris water maze test

A circular pool (100 cm in diameter) filled with white colored water was used for this test. During the hidden platform training, the platform (10 cm in diameter) was submerged in the same position of the pool. Mice underwent four trials of training per day (1 hour interval) for 8 days (day 1-5 and day 7-9). Mice were put into the pool from all of the four quadrants in a pseudorandom manner. During the 60 s training period, mice that reached the hidden platform were left on the platform for 20 s, while mice that were unable to find the platform were guided to it by experimenter's hand and were allowed to stay there for 20 s. The latency to reach the platform, the immobility time, and the swimming speed were measured during each training day. On day 6 and day 10, the mice were subjected to a 60 s probe trial without the platform, during which the number of crossing the platform position were counted. Swimming of mouse was monitored and analyzed with TimeMWM software (O'Hara & Co, Japan).

Fear conditioning test

This test consisted of three trials: conditioning (Day 1), context test (Day 2), and cued test (Day 3). Fear conditioning was performed in a clear plastic chamber (34 × 25 × 28 cm, W x D x H) with a stainless-steel grid floor connected to a shock generator. Animal behavior was recorded with a digital camera which was mounted on the ceiling of the sound-attenuated chamber. White noise (55 dB) was supplied in a sound attenuated chamber as a background noise during each trial. During conditioning trial, mice were placed in the conditioning chamber for 5 min, in which CS (65 dB pure tone) - US (foot-shock: 0.5 mA, 2 s duration) pairing was presented three times. The US was administered at the end of the 30 s CS presentation. The CS-US paring was started at 120, 180, and 240 s in the 5-min conditioning trial. Twenty-four hours after the conditioning trial, a contextual fear test was performed in the same conditioning chamber for 3 min without the CS-US presentation. A cued fear test was performed in an alternative context (white and triangular shape chamber with bedding material same as the home-cage), in which mice were placed for 5 min and given 2-min CS presentation from 120 s of the 5-min trial without any foot shock. The percentage of freezing response (immobility, except for respiration and heart-beat) of mice was calculated with TimeFZ2 software (O'Hara & Co, Japan).

QUANTIFICATION AND STATISTICAL ANALYSIS

All of the data were analyzed with EZR (Saitama Medical Center, Jichi Medical University, Saitama, Japan), which is a graphical user interface for R (The R Foundation for Statistical Computing, Vienna, Austria) and GraphPad Prism software (GraphPad software, USA). EZR is a modified version of R to analyze data more frequently (Kanda, 2013). The data were represented as mean ± SEM. The normality of distribution was assessed by the Kolmogorov-Smirnov test. Student's t test and paired t test were performed when the data showed normal distribution. For comparison of data from two independent samples that did not show normal distributions, Mann-Whitney *U* test was performed. For comparison of data from more than three independent samples that did not show normal distributions, Kruskal-Wallis test followed by Steel-Dwass post hoc analysis was performed. For comparison of data from multiple samples that show normal distributions, ANOVA was performed. In particular, 2-way repeated-measures ANOVA was used to compare data obtained from two mouse groups and recorded multiple times or under multiple experimental conditions. Bonferroni method was used to correct for post hoc multiple comparisons. Statistically significant level was set at $p < 0.05$.